Multi-State Constraint Multipath-Assisted Positioning and Mismatch Alleviation

Xueting Xu, Ao Peng, *Member, IEEE,* Xuemin Hong, *Member, IEEE,* Yixiong Zhang, *Member, IEEE,* Xiao-Ping Zhang, *Fellow, IEEE*

***Abstract*—Multipath propagation greatly affects the accuracy of time of arrival (ToA)-based indoor positioning when line-of-sight (LOS) signals are only used. In this paper, we present a novel real-time and low computation complexity multipath-assisted ToA positioning method, namely MSC-MAP. The delays of reflected signals are taken as additional spatial observations to compensate for an insufficient number of physical transmitters to locate a moving user equipment (UE). Virtual anchors are used to model the propagation path of reflected signals, whose locations are obtained via a multi-state constraint estimator, along with the trajectory of UE. In addition, we demonstrate the mismatch problem in data association and its impact on positioning performance. To achieve real-time processing, we propose two robust multipath-assisted positioning methods with mismatch alleviation by randomly selecting subset and constraint relaxation respectively, to meet various computational complexity requirements. Simulation results show that, for the MSC-MAP method, the mean square error of the position is generally less than 0.2 m in challenging indoor environments. Among mismatch alleviation algorithms, positioning error is reduced by 69% even when the percentage of mismatched measurement data is as high as 42%. The proposed algorithms can also efficiently handle signals with non-Gaussian impairments, a common characteristic in real-world data. Moreover, these algorithms can substantially improve positioning performance while adding minimal computation time in the presence of measurement mismatches, outperforming state-of-the-art methods utilizing different data association techniques.**

***Index Terms*—Multipath-assisted positioning, multi-state constraint, minimum observation constraint, data association, mismatch alleviation.**

I. Introduction

VARIOUS location-based applications supported by traditional global navigation satellite systems are mostly restricted to outdoor scenarios [1]. In the context of indoor positioning, many short-range wireless communication systems, such as Wi-Fi [2], Bluetooth [3], and ultra-wideband [4], have been embraced. While these systems offer absolute positioning capabilities, they often grapple with constraints like limited coverage, sparse infrastructure, and potential interference in the Industrial Scientific Medical band. Compared with short-range wireless communication systems, commercial cellular networks, especially the 5^{th} generation (5G) new radio, stand out due to their widespread infrastructure coverage and effective interference management, thus offering a promising solution for universal indoor positioning services [5].

Some angular-based indoor positioning methods are proposed in [6], [7], but the accuracy is greatly affected by the size of the antenna array. So, distance-based positioning remains the most promising means to achieve high accuracy indoor positioning. However, the positioning accuracy is sensitive to the presence of multipaths [8]. Conventional distance-based localization involves measuring the time delay of the line-of-sight (LOS) path [9], which can easily be obscured by indoor obstacles. Moreover, non-light-of-sight (NLOS) paths can compromise the delay measurement of a LOS path due to limited bandwidth. The multipath phenomenon is thus frequently deemed a hindrance to high-accuracy indoor localization [10]. To eliminate errors induced by NLOS signals in indoor positioning, a straightforward method entails identifying the NLOS components in measurements to prevent them from being used in positioning [11]–[14]. However, the identification probability is often limited in dense multipath scenarios. One misidentification may lead to severe positioning errors. Another classic method mitigates the effects of NLOS measurements on positioning results [15]–[18]. An estimator for the LOS time of arrival (ToA) in multipath conditions is presented in [19] by obtaining an approximate distribution for the received signals of all the antennas. However, the accuracy deteriorates due to the multipath effect. Moreover, it also requires sufficient anchors to achieve trilateration positioning.

Multipath-assisted positioning has emerged as a new positioning paradigm and has garnered increasing research interest [20]. This paradigm treats multipaths as beneficial to positioning given their rich information about the environment [21]. In some typical indoor scenes, specular reflections represent the main multipath source, where reflecting surfaces tend to be large smooth planes such as walls, floors, ceilings, and desktops [22]. The multipath signal caused by specular reflection can be modeled as a direct signal between the receiver and a virtual anchor (VA), i.e., the mirror of a transmitter in the environment. Then, the specular reflection signal can be used as a new observation source for positioning. Importantly, the geometric information of VAs should be exploited before using NLOS observations in positioning. The quality of VAs' geometrical distribution knowledge directly determines the contributions of NLOS observations in multipath-assisted

This research was funded by National Key Research and Development Program of China with Grant Number 2018YFB0505200. (Corresponding author: Ao Peng)

Xueting Xu, Ao Peng, Xuemin Hong and Yixiong Zhang are now with the School of Informatics, Xiamen University, Xiamen, Fujian 361005, China (e-mail: xuxueting4728@gmail.com; pa@xmu.edu.cn; xuemin.hong@xmu.edu.cn; zyx@xmu.edu.cn).

Xiao-Ping Zhang is with Tsinghua Berkeley Shenzhen Institute, Shenzhen, China and the Department of Electrical, Computer & Biomedical Engineering, Toronto Metropolitan University, ON M5B 2K3, Canada (e-mail: xpzhang@ieee.org).

positioning [23].

A multipath-assisted positioning algorithm based on the least-square estimator has been proposed in [24], in which the estimation of user equipment's (UE's) and VAs' positions is formulated as an optimization problem. However, it can only deal with stationary nodes. For moving target, methods based on alternating optimization [25], [26] and the Kalman filter [27] or variants thereof [28]–[31] have been proposed. Given nonlinearity in the measurement model, some optimal Bayesian filter-based multipath-assisted positioning algorithms [21], [32]–[40] that propagate the entire posterior distribution of state vectors have been proposed to achieve better accuracy. The heavy computational load of the classical Bayesian filter induced by Monte Carlo techniques for the sampling distribution function has further spawned many technologies, including particle filters [32], [33], message passing [21], [34]–[37], finite set statistics [38], [39], and variational Bayesian inference [40]. The methods presented in [35]–[37] realize SLAM based on the marginal PDFs of the joint posterior PDF. The required marginal PDFs are approximated through the message-passing algorithm on the factor graph. In [38], positions are characterized by their first-order statistical moment, and the conditional PHD is propagated rather than its PDF. These Bayesian SLAM algorithms process the measurements discretely time step by time step and assume a Markovian state dynamic of the moving agent. If the computational resource is infinite, theoretical real-time positioning can be achieved. However, in practice, positioning using algorithms with high computation complexity will encounter estimation lags owing to the limited computational resource of the implementation platform. To our knowledge, no scholars have discerned the minimum observation constraint (MOC) for VA estimation - the minimum requisite observations needed to obtain a converged estimation of VA's location. This information will offer valuable guidance for designing real-time positioning methods. Real-time here encompasses two distinct aspects. One is theoretical real-time, i.e., updating past state without reliance on future information, and the other is low computational complexity to facilitate real-time processing in a limited hardware resource for implementation.

Because different paths cannot be distinguished through data or code modulated on the signal, a prime concern in multipath-assisted positioning is the data association problem (i.e., identifying the VA from which signal measurement originates). A direct way is to formulate the data association as a binary assignment problem to build the one-to-one correspondence between VAs and measurements [30]. The results of simulation to quantify the data association shows that data association mismatch can degrade positioning performance. But the authors do not address it in [30]. Probability-based data association is proposed in [31], [35], [38], [41]–[43]. The authors seek to design a joint estimation scheme including data association, UE's trajectory and VAs' positions. In this case, the joint posterior probability density function (PDF) is solved via recursive Bayesian filtering methods, such as belief propagation [31], [35], [41] or probability hypothesis density filtering [38]. Next, the posterior PDF of every required variable can be obtained by marginalizing the joint PDF. In [35]–[37], [44], the VAs' states are updated by calculating expectations using the evaluated probabilities of all possible association hypotheses between VAs' states and measurements. Similarly, the authors of [38] use the measurements to update the particle weights representing the UE's state by means of probabilities. Probabilistic methods come with several inherent limitations. Firstly, they demand a high level of spatial correlation, which can be challenging to maintain, especially at low sampling rates. This is due to the frequent birth and death of multipath components, resulting in less correlation between states at adjacent moments, and in some cases, even independence. Moreover, when dealing with low-quality measurements, probabilistic methods can suffer from inaccurate association probabilities. This discrepancy can lead to a situation where the probability of an incorrect association surpasses that of a correct one, resulting in what is known as probabilistic mismatch and subsequently deteriorating performance after expectation. Additionally, in probabilistic data association methods, all available data from various VAs is utilized. However, each VA may possess different estimation qualities, and considering all possible association hypotheses of VAs when calculating expectations can lead to performance degradation, especially when the matching relationship is unclear.

Data association can also be solved indirectly with specially designed baseband processing. The parameters of multipath signals received at the UE is tracked in [45], [46] and [47] via baseband estimators. Then, based on the tracking results, the posterior distribution of the UE's and VAs' positions is estimated recursively using some positioning algorithms (e.g., EKF [45], [46], recursive Bayesian filtering [47]). The random sample consensus is used in [45], [46] to initialize the set of measurement inliers, i.e., measurements agree with the initial estimate of the VA's position. Then, the EKF is used to track multipath parameters with inliers, and the UE's position is estimated using tracked parameters. Accurate positioning hinges on two key prerequisites: maintaining tracking continuity and ensuring the correctness of the initial inlier subset. However, maintaining tracking continuity is a challenging task due to the inherently dynamic nature of multipaths, which undergo frequent changes due to their birth and death processes. Furthermore, in some scenarios, the real inliers within the tracking process can undergo significant variations. For instance, when there is a long sampling interval, substantial distances can separate two consecutive trajectory points, and environmental changes may occur. Consequently, measurements used in subsequent epochs may no longer align with the initial inliers associated with VAs. Additionally, mismatches can occur in subsequent epochs when two paths intersect or when tracking is interrupted, leading to substantial positioning errors in the final positioning stage.

In essence, mismatches are an inevitable aspect of the generalized data association process when employing existing multipath-assisted positioning methods. Consequently, the positioning accuracy of prior methods remains highly sensitive to the correct match rate in data association. However, prior research has yet to delve into robust multipath-assisted positioning in the presence of data association mismatches.

In this article, we present a novel real-time multipath-assisted ToA positioning method based on linear expansion of the observation model, named MSC-MAP, to estimate the locations of a moving UE in complex indoor environments in the 5G system. The delays of reflected signals are taken as additional spatial observations to compensate for an insufficient number of physical transmitters. VAs are used to model the propagation path of reflected signals, whose locations are obtained via a multi-state constraint (MSC) estimator. In our method, since we do not map the environment, the VAs' estimates are mainly used to assist UE's positioning. Hence, our proposed algorithm does not depend on the condition of uniqueness mentioned in [25]. Differently, we use estimation quality control of the VA's position to find some VAs in the environment that can be used to assist positioning. Although it is challenging to use estimation quality control in our method to determine a VA's position estimate when several solutions exist, this does not affect our final localization results. We can exclude non-converging VAs from the UE positioning, which just reduces the number of measurements. Similarly, estimate quality control also allows our method to avoid the need for strict specular reflection assumption. We decide whether a VA is available from the aspect of estimation quality. Even if a curved surface exists, we can also exclude the VA corresponding to it. Then we formulate different measurement models over prior estimations for cases where a VA's position is known and unknown. The low-complexity MSC estimator is applied to address estimation divergence due to insufficient observation. The processing delay is only determined by the bunch size of the multi-state. Hence, the real-time positioning can be realized on both the theoretical and implementation levels at each position update. Based on this, we theoretically analyze the MOC for the proposed estimator, which serves as the basis for real-time multipath-assisted positioning.

Mismatch in data association is one of the key factors that cause the deterioration of multipath-assisted positioning accuracy. The solution of optimal mismatch alleviation can only be obtained by brute-force search. To meet the requirement of real-time processing, we introduce the mismatch matrix and formulate the mismatch in data association. To solve the matrix, we propose two robust multipath-assisted positioning methods with mismatch alleviation by randomly selecting subset and constraint relaxation respectively to suit different computational resources. We select a subset of VAs with good estimation quality and small association error in the random subset selection-based algorithm, which provides a swift and sub-optimal solution under light mismatch scenarios. In the constraint relaxation-based algorithm, we set weights to VAs, which offers an approximately optimal solution under severe mismatch scenarios. The proposed methods have the following advantages over the probabilistic method. Firstly, the proposed MSC estimator can maintain the constraint between sampling points, thus keeping a stable positioning performance when the step size increases. Secondly, the hard association for choosing VAs or assigning weights to VAs used in the methods can help to select beneficial VAs. Furthermore, the mismatch at each position update can be alleviated independently in our proposed methods without requiring the multipath to survive long enough to maintain the tracking relationship. Simulation results show that, for the proposed MSC-MAP, the mean square error (MSE) of the position is generally less than 0.2 m in challenging indoor environments. Among mismatch alleviation algorithms, positioning error is reduced by 69% even when the percentage of mismatched measurement data is as high as 42%, significantly improving the performance of multipath-assisted positioning.

Our main contributions are summarized as follows:

1) A novel real-time multipath-assisted ToA positioning method based on the multi-state constraint estimator is proposed to address estimation divergence due to insufficient observation.
2) We use estimation quality control to find some VAs in the environment that can be used to assist positioning without using strict specular reflection assumption.
3) We formulate the mismatch alleviation problem in data association, and propose two mismatch alleviation methods by randomly selecting subset and constraint relaxation respectively to suit different computational resources.
4) The performances of the proposed multipath-assisted approaches are verified by Monte Carlo simulations. We compare the proposed algorithms against different approaches in literature in terms of positioning error and average runtime.

The remainder of this article is organized as follows. Section II formulate the multipath-assisted positioning problem and mismatch in data association. Section III describes the linearized real-time multipath-assisted positioning approach and analyzes the MOC. Section IV formulates the data association mismatch problem and outlines two mismatch alleviation algorithms. Numerical results and a corresponding discussion are reported in Section V. Finally, Section VI concludes this article. Main notations are summarized in Table 1.

II. Problem Formulation

A. Multipath Propagation Model

To use multipath components for positioning, the relationship between the location of UE and the measurable parameters of the multipath signals should be established in advance. We consider a mobile UE with unknown time-varying position $P_{UE,t}$ at epoch t and R base stations (BSs) with known positions $P_{BS,r}, r = 1, ..., R$. The received signal at epoch t is modeled as

$$s_{rx}(t) = \sum_{i=1}^{N(t)} A_i(t)\, s_{tx}\left(t - \tau_t^{(i)}\right) + n(t), \tag{1}$$

where $N(t)$ denotes the number of measurements (i.e., the number of multipaths that can be observed at time t), $A_i(t)$ is the complex amplitude, $\tau_t^{(i)}$ is the delay of the i-th path for $i = 1, \ldots, N(t)$. For simplicity, we always use $i = 1, ..., R$ to denote the LOS component. If LOS is blocked, then $A_i(t) = 0$. $s_{tx}(t)$ is the transmitted signal, and $n(t)$ indicates white Gaussian distributed receiver noise with mean 0 and variance ${\sigma_n}^2$. Note that a new reference signal called positioning reference

TABLE I
NOTATION LIST

$(\cdot)_{i\cdot}$	the i-th row of the matrix
$\bar{\cdot}$	a priori estimate
$\hat{\cdot}$	a posterior estimate
t	epoch
T	number of sequential observation epochs for per position update
$N(t)$, N	number of measurements at epoch t and for T epochs
R	number of base stations
K	number of VAs with a posterior estimates
M	number of unknown VAs
s_{tx}, s_{rx}	transmitted signal and received signal for downlink
A_i	complex amplitude of the i-th multipath
$\tau_t^{(i)}$, $\hat{\tau}_t^{(i)}$	delay of the i-th multipath at epoch t and its estimate
n, $\mathbf{n}$	Gaussian noise and noise vector
$P_{BS,r}$	position of the r-th base station
$P_{UE,t}$	UE position at epoch t
$P_{VA}^{(i)}$	position of the i-th VA
$\hat{\mathbf{P}}$	collection matrix of estimated positions UE and VAs
$d_t^{(i)}$,$\hat{d}_t^{(i)}$	distance between UE and the i-th VA at epoch t, and its estimate
$\Delta\hat{d}_t^{(i)}$, $\Delta\bar{d}_t^{(i)}$	distance measurement residual when a VA's position is known and unknown respectively
$\mathbf{Y}$	joint measurement model of UE and all VAs with sequential epochs
$\mathcal{Y}$	measurement set
$\mathbf{X}$, $\hat{\mathbf{X}}$	location corrections of VAs and UE and its estimate
$\mathbf{H}$, $\hat{\mathbf{H}}$	observation matrix and its estimate
ϕ_i, $\mathbf{\Phi}$	mismatch alleviation sequence and matrix
δ	estimation error generated due to data mismatch
$\mathbf{w}$, $\mathbf{W}$	residual vector of all measurements and its projection matrix without normalized
$\mathbf{w}_t$	residual vector of UE and VAs position at epoch t
$\boldsymbol{\alpha}$, $\mathbf{z}$	selection vector and its intermediate variable
p	residual sum of selected measurements
$\boldsymbol{\nu}$, λ	Lagrange multiplier vector and scalar
ε_A, ε_B	error threshold of proposed two algorithm
d^*	sub-optimal lower bound of original integer program problem
m	number of measurements per selection in RS-subset algorithm
η	mismatch judgment threshold of measurement subset in RS-subset algorithm
l	parameter used to delete mismatched measurements that have been repeatedly selected
$\mathcal{C}$	mismatch alleviated set
ϕ_A, ϕ_B	barrier function for the optimal problem in RS-subset algorithm and CR algorithm
u	constraint on the sum of weights of all measurement values in CR algorithm
t_B	parameters used to determine the quality of the approximation of barrier methods in CR algorithm
$\Delta\boldsymbol{\alpha}$, λ^2	Newton descent direction and decrement
ϵ	tolerance of Newton iteration
β	update step length of inner iteration of CR algorithm
ρ	scale factor of outer iteration of CR algorithm

signal (i.e., PRS) is introduced by 3GPP in TS 38.211 (Release 16) [48] for UEs to perform downlink reference signal time difference (DL-RSTD) measurements at each base station, the delays $\tau_t^{(i)}, i = 1, \ldots, N(t)$ can be estimated with the help of PRS by some channel estimation methods.

For LOS component, $\tau_t^{(r)}$ (for $r \in \{1, ..., R\}$) provide measurements to the distances between the UE and BSs:

$$\tau_t^{(r)} = \frac{1}{c} \left\| P_{UE,t} - P_{BS,r} \right\|, \tag{2}$$

where c is the speed of light. For NLOS components, the propagation delays cannot be used directly because the propagation path is not straight. To achieve multipath-assisted positioning, we use the model of mirror point (i.e., VA) of a transmitter against a reflecting surface [22], as illustrated in Fig. 1. According to geometrical optics theory, the propagation distance from the transmitter to the UE after reflection is equal to the distance from the VA to the UE. With the help of VA, the measurement model of the propagation delay for the i-th multipath component can be expressed as follows,

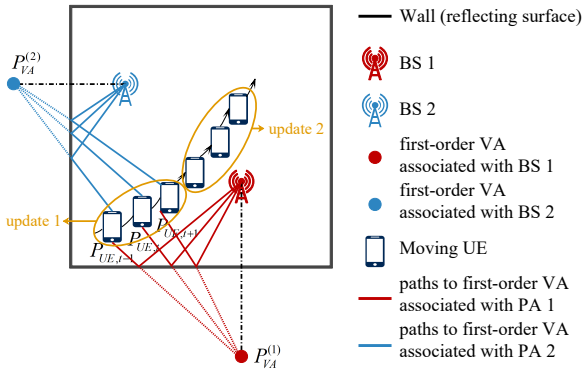

Fig. 1. Example of an environment map with VAs and reflected multipath. The thick black line indicates walls, which we consider to be reflecting surfaces. The BSs at fixed positions are indicated by, respectively, a red base station graphic and a blue one within the floor plan. The UE moves along the thin black line. The red circle and blue one indicate examples of the first-order VAs associated with BS 1 and BS 2, respectively. The red and blue lines show some examples of the first-order reflection paths between the moving UE and two VAs. One orange ellipse indicates one position update using multiple measurement epochs.

$$\tau_t^{(i)} = \frac{1}{c} \left\| P_{UE,t} - P_{VA}^{(i)} \right\|, \tag{3}$$

where $P_{VA}^{(i)}, i = R+1, ..., N(t)$ denotes the position of the i-th VA corresponding to the i-th multipath signal. The BSs can also be regarded as special VAs for the LOS paths, which are recorded as $\{P_{VA}^{(1)}, ..., P_{VA}^{(R)}\}$.

For irregular reflection surfaces, which are common in typical indoor scenarios, we use small segments for approximation. In other words, we can increase the number of VAs used in the model to achieve piecewise approximation of the reflection of irregular surfaces.

B. Multipath-assisted Positioning

The UE receives several multipath signals at one moment. To formularize the observation equation (3), the correspondence between VAs and multipath signals must be determined, (i.e. data association). We use the classical Hungarian algorithm [49] to achieve data association, then the observations are arranged by order of associated VAs.

We record the distance vector between the UE and VAs as $\mathbf{d}_t = \begin{bmatrix} d_t^{(1)} & \cdots & d_t^{(N(t))} \end{bmatrix}^T$, where $d_t^{(i)}$ denotes the distance between the UE and the i-th VA, and

$$d_t^{(i)} = \| \left(\mathbf{1}^T \cdot P_{UE,t} - \begin{bmatrix} P_{VA}^{(1)} & \cdots & P_{VA}^{(N(t))} \end{bmatrix}^T \right)_{i\cdot} \|. \tag{4}$$

$(\cdot)_{i\cdot}$ represents the i-th row of the matrix to consider the dimension of the position. Therefore, residual vector of UE and VAs position at epoch t is

$$\mathbf{w}_t = \mathbf{d}_t - c\begin{bmatrix} \tau_t^{(1)} & \cdots & \tau_t^{(N(t))} \end{bmatrix}^T. \tag{5}$$

Let $\mathbf{P}$ be the position matrix of UE and VAs:

$$\mathbf{P} = \begin{bmatrix} P_{UE,1} & \cdots & P_{UE,T} & P_{VA}^{(1)} & \cdots & P_{VA}^{(M)} \end{bmatrix}^T. \tag{6}$$

The essential problem of multipath-assisted positioning is to estimate the trajectory of UE $P_{UE,t}, t \in \{1, ..., T\}$ and positions of VAs $P_{VA}^{(i)}, i \in \{1, ..., M\}$ simultaneously with known $\boldsymbol{\tau}_t, t = 1, \ldots, T$, where $\boldsymbol{\tau}_t = [\tau_t^{(1)} \cdots \tau_t^{(N(t))}]$. Based on the idea of least square method, we realize multipath-assisted positioning by minimizing the residual sum of squares during the UE movement, that is:

$$\hat{\mathbf{P}} = \arg\min_{\hat{\mathbf{P}}} \sum_{t=1}^{T} \|\mathbf{w}_t\|^2. \tag{7}$$

We start by assuming that the DA algorithm used in this paper can obtain ideal match results. In the next section, we propose a novel multipath-assisted positioning method based on the MOC with real-time capability and low computational complexity.

C. Mismatch in Data Association

Mismatches in data association are unavoidable due to measurement noise and the uncertainty of VAs' geometric information. According to (4)-(5), a mismatch will lead to disorder between ToA measurements and VAs, resulting in disordered propagation model and even severe positioning error. Therefore, it is thus crucial to ensure positioning performance of $P_{UE,t}$ and $P_{VA}^{(i)}, i \in \{1, ..., N(t)\}$ even in the presence of mismatches.

We define a data association alleviation sequence $\{\phi_i = j; 1 \le i \le N(t), 1 \le j \le N(t)\}$, meaning that the i-th ToA measurements are reassociated with the j-th VA. As such, $\phi_i = i$ indicates that the original allocation of i-th measurement will not be changed. The mismatch alleviation matrix is defined as $\mathbf{\Phi}_t \in \mathbb{R}^{N(t)\times N(t)}$, where each element $(\mathbf{\Phi}_t)_{ij}$ takes the value

$$(\mathbf{\Phi}_t)_{ij} = \begin{cases} 1, \phi_i = j, \\ 0, \phi_i \neq j, \end{cases} \tag{8}$$

where $(\cdot)_{ij}$ represents the element of the i-th row and j-th column of the matrix. Only one non-zero element in each row and column of $\mathbf{\Phi}_t$ takes the value 1 and $\mathbf{\Phi}_t^{-1} = \mathbf{\Phi}_t^T$. When no mismatch is present, $\mathbf{\Phi}_t = \mathbf{I}$. Let $\mathbf{\Phi}$ be the diagonal matrix consisting of mismatch alleviation matrix for T epochs, i.e., $\mathbf{\Phi} = diag\,[\mathbf{\Phi}_1 \cdots \mathbf{\Phi}_T]$.

We assume that the estimated position matrix of UE and VAs is $\hat{\mathbf{P}}$ with mismatch. The goal of data association mismatch alleviation is to estimate $\mathbf{\Phi}$ by minimizing the error between $\hat{\mathbf{P}}$ and $\mathbf{P}$, that is:

$$\mathbf{\Phi} = \arg\min_{\mathbf{\Phi}} \sum_{t=1}^{T} \|\hat{\mathbf{P}}(\mathbf{\Phi}) - \mathbf{P}\|^2. \tag{9}$$

Mismatch alleviation algorithms are discussed in depth in Section IV.

III. Real-time Multipath-Assisted Positioning Method

In this part, we propose a real-time MSC multipath-assisted positioning method, namely MSC-MAP, to jointly estimate the UE's and VAs' positions. We first give measurement models based on Taylor expansion according to prior knowledge of a VA's position. Then we use the MSC to ensure convergence of the position estimates, followed by the description of the minimal requirement of observations for joint position estimation, which we call the MOC. Finally, we give the estimated positions of the UE and VAs via the joint measurement model with MOC.

A. Linear Expansion of the Observation Model

We adopt ToA-only positioning, in which positions are calculated using distances between the UE and VAs estimated by the delay measurements of received signals. The distance measurement model at epoch t can be written as

$$\begin{aligned} \hat{d}_t^{(i)} = c\hat{\tau}_t^{(i)} &= \left\| P_{UE,t} - P_{VA}^{(i)} \right\| + n(t) \\ &\triangleq f\left(P_{UE,t}, P_{VA}^{(i)}\right) + n(t), \end{aligned} \tag{10}$$

where $\hat{d}_t^{(i)}$ denotes the estimate of $d_t^{(i)}$, and $\hat{\tau}_t^{(i)}$ denotes the estimated propagation path delay from the i-th VA.

The visibility of VAs varies due to the complicated obstacles in an indoor environment. Visible VAs' number in each epoch is determined by received multipath signals number. We use a set to record all the observed VAs. A new VA is added to the set whenever a new multipath signal is received. We use the multipath delay difference between adjacent epochs to determine whether a new multipath signal has been observed. We classify VAs into known and unknown VAs based on the convergence of the position estimates of VAs. We draw the idea of receiver autonomous integrity monitoring (RAIM) to judge the convergence. When the ToA residual obtained by applying the estimated VA's position is less than the threshold we set for RAIM, the estimate is converged, and this VA is decided as a known VA.

When the position estimates of the VAs are unknown, given an a priori estimate of the i-th VA position $\overline{P}_{VA}^{(i)}$, we can linearize the $\hat{d}_t^{(i)}$ with respect to $\overline{P}_{UE,t}$ and $\overline{P}_{VA}^{(i)}$ using Taylor expansion, obtaining

$$\begin{aligned} \hat{d}_t^{(i)} = f\left(\overline{P}_{UE,t}, \bar{P}_{VA}^{(i)}\right) &+ \left.\frac{\partial f}{\partial P_{UE,t}}\right|_{\overline{P}_{UE,t}} \Delta P_{UE,t} \\ &+ \left.\frac{\partial f}{\partial P_{VA}^{(i)}}\right|_{\overline{P}_{VA}^{(i)}} \Delta P_{VA}^{(i)} + o\left(\Delta P_{UE,t} \Delta P_{VA}^{(i)}\right), \end{aligned} \tag{11}$$

where $\Delta P_{VA}^{(i)} = P_{VA}^{(i)} - \bar{P}_{VA}^{(i)}$ is the location correction of the i-th VA. $o\left(\Delta P_{UE,t}\Delta P_{VA}^{(i)}\right) = o\left(\left(\Delta P_{UE,t}\right)^2 + \left(\Delta P_{VA}^{(i)}\right)^2\right)$.

After the VAs' position estimates have converged, we define that VAs' positions are known. We assume the position of the

i-th VA is $\hat{P}_{VA}^{(i)}$ and the a priori estimate of UE is $\overline{P}_{UE,t}$ in epoch t. In this instance, $P_{VA}^{(i)} = \hat{P}_{VA}^{(i)}$. In linearizing the distance measurement model with respect to $\overline{P}_{UE,t}$, we can obtain

$$\begin{aligned} \hat{d}_t^{(i)} = f\left(\overline{P}_{UE,t}, \hat{P}_{VA}^{(i)}\right) + \left.\frac{\partial f}{\partial P_{UE,t}}\right|_{\overline{P}_{UE,t}} \Delta P_{UE,t} \\ + o\left(\Delta {P_{UE,t}}^2\right), \end{aligned} \tag{12}$$

where $\Delta P_{UE,t} = P_{UE,t} - \overline{P}_{UE,t}$ is the location correction of the UE at epoch t.

For convenience, we record the distance measurement residual as $\Delta\hat{d}_t^{(i)} = \hat{d}_t^{(i)} - f\left(\overline{P}_{UE,t}, \hat{P}_{VA}^{(i)}\right)$ when a VA's position is known and as $\Delta\bar{d}_t^{(i)} = \hat{d}_t^{(i)} - f\left(\overline{P}_{UE,t}, \bar{P}_{VA}^{(i)}\right)$ when its position is unknown. Let

$$\mathbf{v}_t^i = \left.\frac{\partial f}{\partial P_{VA}}\right|_{\overline{P}_{VA}^{(i)}}, \mathbf{u}_t^i = \left.\frac{\partial f}{\partial P_{UE,t}}\right|_{\overline{P}_{UE,t}} = \begin{cases} \overline{\mathbf{u}}_t^i, \text{for Case 1,} \\ \widehat{\mathbf{u}}_t^i, \text{for Case 2.} \end{cases} \tag{13}$$

With unknown VAs positions, the measurement model at epoch t is

$$\begin{aligned} &\left[\begin{array}{cccc} \Delta\bar{d}_t^{(1)} & \cdots & \Delta\bar{d}_t^{(M)} \end{array}\right]^T \\ &= \left[\begin{array}{cccc} \overline{\mathbf{u}}_t^1 & \mathbf{v}_t^1 & \cdots & \mathbf{o} \\ \vdots & \vdots & \ddots & \vdots \\ \overline{\mathbf{u}}_t^M & \mathbf{o} & \cdots & \mathbf{v}_t^M \end{array}\right]_{M\times 2(M+1)} \\ &\times \left[\begin{array}{cccc} {\Delta P_{UE,t}}^T & {\Delta P_{VA}^{(1)}}^T & \cdots & {\Delta P_{VA}^{(M)}}^T \end{array}\right]_{2(M+1)\times 1}^T, \end{aligned} \tag{14}$$

where M denotes the number of measurements corresponding to VAs with unknown positions.

With known VAs positions, the measurement model is described as

$$\left[\begin{array}{ccc} \Delta\hat{d}_t^{(1)} & \cdots & \Delta\hat{d}_t^{(K)} \end{array}\right]^T = \left[\begin{array}{ccc} \widehat{\mathbf{u}}_t^1 & \cdots & \widehat{\mathbf{u}}_t^K \end{array}\right]_{K\times 2}^T \Delta P_{UE,t}, \tag{15}$$

where K is the number of measurements corresponding to VAs with a posterior estimates.

For convenience, we let

$$\Delta\bar{\mathbf{d}}_t = \left[\begin{array}{ccc} \Delta\bar{d}_t^{(1)} & \cdots & \Delta\bar{d}_t^{(M)} \end{array}\right]^T, \tag{16a}$$

$$\Delta\widehat{\mathbf{d}}_t = \left[\begin{array}{ccc} \Delta\hat{d}_t^{(1)} & \cdots & \Delta\hat{d}_t^{(K)} \end{array}\right]^T, \tag{16b}$$

B. Real-time Multipath-Assisted Positioning Based on Multi-state Constraint

We consider positioning in a two-dimensional scene which can be easily expanded to a three-dimensional scene. For two-dimensional positioning with an unknown VA, the dimension of the observation matrix of (14) is $M \times 2(M+1)$. Therefore, the observation matrix is non-full rank with a linear correlation column vector group, leading to insufficient observations for a single epoch. The constraint of a single observation to the position estimation is therefore weak and may easily induce divergence due to observation noise. To rectify this problem, we consider a MSC [50], [51] (i.e., sequential observations) to jointly estimate the locations of VAs and the UE. Because each position update is independent and similar, we present the algorithm with a single position estimating step as an example.

We use the ToA measurement model with T sequential epochs. Suppose there are M unknown VA's with M measurement model for case 1 and K known VA's with K ones for case 2 during T epochs. We assume that N is the total number of measurements for T epochs used for one position update. Accordingly, $N = T(M+K)$. The joint measurement model of the $(M+K)$ VAs with T epochs can be written as

$$\begin{aligned} \mathbf{Y} &= \left[\begin{array}{cccccc} \Delta\bar{\mathbf{d}}_1{}^T & \cdots & \Delta\bar{\mathbf{d}}_T{}^T & \Delta\widehat{\mathbf{d}}_1{}^T & \cdots & \Delta\widehat{\mathbf{d}}_T{}^T \end{array}\right]^T \\ &= \left[\begin{array}{cccc} \overline{\mathbf{U}}_1 & \cdots & \mathbf{O} & \mathbf{V}_1 \\ \vdots & \ddots & \vdots & \vdots \\ \mathbf{O} & \cdots & \overline{\mathbf{U}}_T & \mathbf{V}_T \\ \widehat{\mathbf{U}}_1 & \cdots & \mathbf{O} & \mathbf{O} \\ \vdots & \ddots & \vdots & \mathbf{O} \\ \mathbf{O} & \cdots & \widehat{\mathbf{U}}_T & \mathbf{O} \end{array}\right]_{T(M+K)\times 2(M+T)} \mathbf{X} = \mathbf{H}\mathbf{X}, \end{aligned} \tag{17}$$

where

$$\overline{\mathbf{U}}_t = \left[\begin{array}{ccc} \overline{\mathbf{u}}_t^1{}^T & \cdots & \overline{\mathbf{u}}_t^M{}^T \end{array}\right]^T, \widehat{\mathbf{U}}_t = \left[\begin{array}{ccc} \widehat{\mathbf{u}}_t^1{}^T & \cdots & \widehat{\mathbf{u}}_t^K{}^T \end{array}\right]^T, \tag{18}$$

$$\mathbf{V}_t = \left[\begin{array}{ccc} \mathbf{v}_t^1 & \cdots & \mathbf{o} \\ \vdots & \ddots & \vdots \\ \mathbf{o} & \cdots & \mathbf{v}_t^M \end{array}\right], \tag{19}$$

$$\mathbf{X} = \left[\begin{array}{cccc} {\Delta P_{UE,1}}^T \cdots {\Delta P_{UE,T}}^T & {\Delta P_{VA}^{(1)}}^T \cdots {\Delta P_{VA}^{(M)}}^T \end{array}\right]^T. \tag{20}$$

$\mathbf{X}$ is the location corrections of VAs and UE.

The dimension of the observation matrix $\mathbf{H}$ of (17) is $T(M+K) \times 2(M+T)$. Clearly, (17) has one and only one solution because the calculated UE's and VAs' positions are unique, meaning that the observation matrix is full column rank:

$$T \times (M+K) \geq 2(M+T). \tag{21}$$

The above formula provides the MOC for solving (17). For example, when $K = 0$ and $M = 5$, $T \geq 4$ can guarantee that (17) has a solution.

Equation (21) serves as a reference for determining the sequential epochs within the estimator for real-time positioning. The number of epochs T is the number of observation instances used for one position update, that is, a fraction of discrete time instances. The selection of the number of epochs can be tailored with flexibility based on the guidance provided by (21). The relationship between one position update and the number of measurement epoch is visually shown in Fig. 1.

When the number of observation epochs satisfies the MOC (21), a solution of (17) is available based on the least squares criterion:

$$\hat{\mathbf{X}} = (\hat{\mathbf{H}}^T\hat{\mathbf{H}})^{-1}\hat{\mathbf{H}}^T\mathbf{Y}, \tag{22}$$

where $\hat{\mathbf{H}}$ is the estimated observation matrix. The positions of the UE and VAs estimated via joint position estimation with a MSC are then

$$\hat{\mathbf{P}} = \hat{\mathbf{X}} + \begin{bmatrix} \bar{P}_{UE,1} & \cdots & \bar{P}_{UE,T} & \bar{P}_{VA}^{(1)} & \cdots & \bar{P}_{VA}^{(M)} \end{bmatrix}^T. \tag{23}$$

For each estimation, when N measurements are received, we obtain the linearized measurement model according to (17)-(20) and then apply (22) and (23) to estimate the positions of UE and VAs. In the MSC-MAP method, a position update is performed every T measurement epochs. We do not need to update positions with future data, and the processing delay is determined by T only. In addition, the MSC-MAP method has low complexity. Therefore, the MSC-MAP method can be considered real-time on both the theoretical and implementation levels at each position update.

We can realize the estimate quality control of VA's position by judging the convergence of VA. When a VA's position is still unknown after multiple position updates, the estimate quality of this VA's position is poor and the estimate cannot converge, which may be caused by scatterers or non-specular reflections. We can exclude these non-converged VAs in the subsequent position updates.

It should be noted that the least square is used to explore the distinct constraint of the observation epoch during real-time state estimation. Upon adding the kinematic model of the UE to the linearized observation model (17), joint position estimation can be easily extended to some filter methods; this topic is beyond the scope of this paper.

IV. Data Association Mismatch Alleviation Approach

We first formulate the mismatch problem. Then, to meet the requirement of real-time processing, two mismatch alleviation algorithms are proposed to fulfill distinct computational load and accuracy requirements.

A. Mismatch Alleviation Problem

As stated in section II-C, to achieve joint position estimation of VAs and the UE, it is essential to recover the observation matrix $\mathbf{H}$ in the correct association order. When the ideal data association can be obtained, the row of the measurement matrix $\mathbf{H}$ (17) corresponding to every $\Delta\bar{\mathbf{d}}_t^{(i)}$ (or $\Delta\hat{\mathbf{d}}_t^{(i)}$) should be $\overline{\mathbf{u}}_t^i$ and $\mathbf{v}_t^i$ (or $\widehat{\mathbf{u}}_t^i$). However, with a mismatch in the data association, the ToA measurement corresponding to the i-th VA is wrongly associated with the j-th VA, turning the row of $\mathbf{H}$ corresponding to $\Delta\bar{\mathbf{d}}_t^{(i)}$ (or $\Delta\hat{\mathbf{d}}_t^{(i)}$) into $\overline{\mathbf{u}}_t^j$ and $\mathbf{v}_t^j$ (or $\widehat{\mathbf{u}}_t^j$). This outcome will further lead to a mismatch of the j-th ToA measurements.

Considering the mismatch in data association, the measurement model becomes

$$\mathbf{Y} = \mathbf{\Phi}\hat{\mathbf{H}}\mathbf{X} + \mathbf{n}, \tag{24}$$

where $\hat{\mathbf{H}}$ denotes the estimated observation matrix derived from data association results; and $\mathbf{n}$ denotes the Gaussian distributed noise vector with mean 0 and covariance matrix $\mathbf{Q}$, assuming that the observation noise of different paths is irrelevant. When no mismatch is present, $\hat{\mathbf{H}} = \mathbf{H}$.

Based on the preceding section, $\hat{\mathbf{H}}$ is full column rank. Therefore, $\hat{\mathbf{H}}^T\hat{\mathbf{H}}$ is a non-singular matrix. The least squares estimation of $\mathbf{X}$ by applying the mismatch alleviation matrix to the observation model can be calculated as

$$\mathbf{X} = \left[\left(\mathbf{\Phi}\hat{\mathbf{H}}\right)^T\left(\mathbf{\Phi}\hat{\mathbf{H}}\right)\right]^{-1}\left(\mathbf{\Phi}\hat{\mathbf{H}}\right)^T\mathbf{Y} = (\hat{\mathbf{H}}^T\hat{\mathbf{H}})^{-1}\hat{\mathbf{H}}^T\mathbf{\Phi}^T\mathbf{Y}. \tag{25}$$

Accordingly, an estimation error is generated due to the mismatch, namely

$$\delta = \mathbf{X} - \hat{\mathbf{X}} = (\hat{\mathbf{H}}^T\hat{\mathbf{H}})^{-1}\hat{\mathbf{H}}^T\left(\mathbf{\Phi}^T - \mathbf{I}\right)\mathbf{Y}. \tag{26}$$

Naturally, δ includes a non-zero-mean bias; that is, severe positioning error exists in some part of the UE's trajectory due to mismatch.

The $\mathbf{\Phi}$ is essentially an adjustment of the data association results. We can get the correct association by finding the optimal $\mathbf{\Phi}$ under any unordered association. However, $\mathbf{\Phi}$ has a total of $N!$ possible values. The best solution of $\mathbf{\Phi}$ can only be obtained by a brute-force search. Therefore, it is necessary to develop fast mismatch alleviation algorithms.

B. Randomly Selecting Subset (RS-Subset)-Based Mismatch Alleviation

We propose a mismatch alleviation algorithm, namely RS-Subset, by randomly evaluating some small-scale subsets and then finding a mismatch-free subset with the desired size to obtain the final solution.

We use the posterior residual to evaluate the mismatch alleviation matrix $\mathbf{\Phi}$ and estimated correction matrix $\hat{\mathbf{X}}$. Specifically, the residual vector of all measurements is

$$\mathbf{w} = \mathbf{Y} - \hat{\mathbf{H}}\hat{\mathbf{X}} = [\mathbf{I} - \hat{\mathbf{H}}(\hat{\mathbf{H}}^T\hat{\mathbf{H}})^{-1}\hat{\mathbf{H}}^T]\mathbf{Y}. \tag{27}$$

When no mismatch occurs, the posterior residual vector follows a joint Gaussian distribution with zero mean. The estimated bias induced by the mismatch can cause non-zero bias in the means of corresponding residuals. We can thus use the residual sum to assess the quality of the final joint position estimates of both the UE and VAs.

We define a *selection vector* $\boldsymbol{\alpha} = [\alpha_1, ..., \alpha_N]^T$, whose i-th entry is $\alpha_i = 0$ if the i-th measurement is excluded from the positioning solution and $\alpha_i = 1$ if it is selected in the positioning solution. Therefore, the ideal way to achieve mismatch alleviation is to find an optimal selection vector and then use a subset of measurements to complete joint position estimation. To avoid repeating the entire positioning procedure, we use the chosen residual sum $p = \boldsymbol{\alpha}^{\mathrm{T}}\mathbf{w}$ to evaluate the quality of the final estimate.

Then, we can define an optimization problem as minimizing the absolute value of the selected residual sum. To effectively solve this problem, we convert it to minimize the squared sum of residuals, wherein

$$\min_{\boldsymbol{\alpha}} p^2 = \left(\boldsymbol{\alpha}^T\mathbf{w}\right)^2 = \left(\boldsymbol{\alpha}^T\mathbf{w}\right)\left(\boldsymbol{\alpha}^T\mathbf{w}\right). \tag{28}$$

Because $\boldsymbol{\alpha}^T\mathbf{w}$ is a scalar, we have $\boldsymbol{\alpha}^T\mathbf{w} = \mathbf{w}^T\boldsymbol{\alpha}$. Let $\mathbf{W} = \mathbf{w}\mathbf{w}^T$; the mismatch alleviation optimization problem with constraints can be written as

$$\min_{\boldsymbol{\alpha}} \quad \boldsymbol{\alpha}^T\mathbf{W}\boldsymbol{\alpha} \tag{29}$$

$$\text{s.t.} \quad \alpha_i \in \{0,1\}, \qquad \forall i \in \{1,...,N\} \tag{30}$$

$$\sum_i \alpha_i \geq 2(M+T), \quad \forall i \in \{1,...,N\}. \tag{31}$$

Constraints (31) represents that the number of selected measurements need to satisfy the MOC (21).

As displayed in (29)-(31), the mismatch alleviation problem is a 0-1 integer programming problem. Therefore, we use approximation algorithms to obtain a relatively good solution to this problem quickly.

The algorithm is split into two steps. In the first step, a ε_A sub-optimal lower bound of the original problem is obtained by solving the Lagrange dual problem, which can provide a reliable guideline for evaluating the subset in the subsequent step. In the second step, we use the lower bound to determine whether mismatched data exist in a randomly selected subset of measurements. Next, we merge several subsets without mismatches to obtain the final subset used for positioning.

We first find a ε_A sub-optimal lower bound of the original problem. For the convenience of a symmetrical value domain in the optimization problem, we define an intermediate variable $\mathbf{z} = 2\left(\boldsymbol{\alpha} - \frac{1}{2}\right)$, then $z_i \in \{-1,1\}, \forall i \in \{1,...,N\}$. The optimal problem (29) can be rewritten as

$$\min_{\mathbf{z}} \quad \mathbf{z}^T\mathbf{W}\mathbf{z} \tag{32}$$

$$\text{s.t.} \quad z_i \in (-1,1), \qquad \forall i \in \{1,...,N\}, \tag{33}$$

$$\sum_i (z_i+1) \geq 4(M+T), \quad \forall i \in \{1,...,N\}. \tag{34}$$

Although (32) is not convex, the dual function of (32) is concave because it is the pointwise infimum of a family of affine functions. In this case, we can obtain a lower bound of (32) using the dual function.

According to [52], the Lagrange dual problem associated with the problem (32) is

$$\min_{\boldsymbol{\nu}} \quad \mathbf{1}^T\boldsymbol{\nu} \tag{35}$$

$$\text{s.t.} \quad -\mathbf{W} - \mathbf{diag}(\boldsymbol{\nu}) \preceq 0, \tag{36}$$

where $\boldsymbol{\nu}$ is Lagrange multiplier vector and $\mathbf{diag}(\cdot)$ represents diagonal matrix. Problem (35) is a semidefinite program in inequality form, which can be solved via the barrier method.

Using the generalized logarithm $\log\det\mathbf{X}$, we have the barrier function for problem $\phi_A(\boldsymbol{\nu}) = -\log\det|\mathbf{W} + \mathbf{diag}(\boldsymbol{\nu})|$ with $\mathbf{dom}\phi_A = \{\boldsymbol{\nu}\,|\mathbf{W} + \mathbf{diag}(\boldsymbol{\nu}) \succ 0\}$. Problem (35) can be approximately formulated as

$$\min_{\boldsymbol{\nu}} \quad \frac{1}{\varepsilon_A}\left(\mathbf{1}^T\boldsymbol{\nu}\right) - \log\det|\mathbf{W} + \mathbf{diag}(\boldsymbol{\nu})|, \tag{37}$$

where $\varepsilon_A > 0$ is the parameter used to determine the quality of the approximation, which improves as ε_A decreases. For a strictly feasible $\boldsymbol{\nu}$, the gradient of $\phi_A(\boldsymbol{\nu})$ is

$$\frac{\partial\phi_A(\boldsymbol{\nu})}{\partial\nu_i} = -\mathrm{tr}\left\{[\mathbf{W} + \mathbf{diag}(\boldsymbol{\nu})]^{-1}\frac{\partial\mathbf{diag}(\boldsymbol{\nu})}{\partial\nu_i}\right\}, \quad \forall i \in \{1,...,N\}, \tag{38}$$

where

$$\frac{\partial\mathbf{diag}(\boldsymbol{\nu})}{\partial\nu_i} = \mathbf{diag}\left(e_1, e_2, ..., e_n\right), \forall i \in \{1,...,N\}, \tag{39}$$

$$e_j = \begin{cases} 1, j = i \\ 0, j \neq i \end{cases}, \forall j \in \{1,...,N\}. \tag{40}$$

Therefore, the optimality conditions of (37) obtained from the gradient are

$$I\left(\nu_i^*\right) = \frac{1}{\varepsilon_A} + \frac{\partial\phi_A(\boldsymbol{\nu}^*)}{\partial\nu_i} = 0, \forall i \in \{1,...,N\}. \tag{41}$$

Let $\mathbf{A} = [\mathbf{W} + \mathbf{diag}(\boldsymbol{\nu}^*)]^{-1} = [a_{ij}]_{N\times N}$; then, we have

$$I\left(v_i^*\right) = 1/\varepsilon_A - a_{ii} = 0, \forall i \in \{1,...,N\}. \tag{42}$$

For any $\varepsilon_A > 0$, the optimal solution $\boldsymbol{\nu}^*$ of (37) can be found from (42). As such, let ε_A an error threshold, we can acquire the ε_A sub-optimal solution of (35). Additionally, the ε_A sub-optimal lower bound d^* for the optimal solution p^* of the original problem (32) can be obtained by $d^* = -\mathbf{1}^T\boldsymbol{\nu}^*$. Although there is a duality gap between p^* and d^* due to the non-convexity of (32) (i.e., $p^* > d^*$), d^* can still provide a reliable guideline for randomly selecting a subset in the next step.

Then, we use d^* to evaluate the quality of selected subsets, and then compose a final selection with specified size. According to the union set, we can determine the mismatch alleviation matrix $\boldsymbol{\Phi} = \boldsymbol{\alpha}\boldsymbol{\alpha}^T$ via selection vector $\boldsymbol{\alpha}$. The modified correction matrix is

$$\hat{\mathbf{X}} = (\hat{\mathbf{H}}^T\hat{\mathbf{H}})^{-1}\hat{\mathbf{H}}^T\boldsymbol{\Phi}^T\mathbf{Y}. \tag{43}$$

Finally, we can obtain the estimated positions of UE and VAs (i.e., $\hat{\mathbf{P}}$) according to (23).

The detailed process is presented in Algorithm 1. We set a mismatch judgment threshold $\eta = d^*(\varepsilon_A)$ (Line 4). When the cardinality of the correctly matched measurement set $\mathcal{C}$ (denoted by $|\mathcal{C}|$) is less than $2(T+M)$ (i.e., the set size under the MOC), $m(m < n)$ measurements are randomly selected from the set $\mathcal{Y} = [y_1, y_2, ..., y_n]^T$ of observations to form subsets $\mathcal{B}_k$, where $k = \{1, 2, ...\}$ (Line 7). $z_i(i \in \{1, 2, ..., n\})$ corresponding to the measurements in $\mathcal{B}_k$ are equal to 1; otherwise, $z_i = -1$ (Lines 8 - 12). Afterwards, we calculate the average of the squared sum of the residual $r_{\mathcal{B}_k}$ of selected measurements according to the selection vector $z_{\mathcal{B}_k}$ of $\mathcal{B}_k$ (Line 13). If $r_{\mathcal{B}_k} \leq \eta$, we assume that none of the measurements in the k-th subset are mismatched and thus put the elements of $\mathcal{B}_k$ into $\mathcal{C}$; if $r_{\mathcal{B}_k} > \eta$, then $\mathcal{B}_k$ has mismatched measurements. When an identical measurement y_i appears in l data mismatch subsets, y_i is considered as a mismatched measurement, which is deleted from the $\mathcal{Y}$ to decrease the possibility of selecting a mismatched measurement in a subsequent step (Line 17 - 20). When the number of elements in $\mathcal{C}$ exceeds $2(T+M)$, we use $\mathcal{C}$ as the final selected subset to estimate the positions of UE and VAs.

Algorithm 1: RS-subset (randomly selecting subsets) algorithm.

Input: Estimated measurement matrix $\hat{\mathbf{H}}$, measurement epoch T, number of unknown VA M, measurements matrix $\mathbf{Y}$, parameters ε_A, N, m, and l

Output: Mismatch alleviated set $\mathcal{C}$ and estimated positions $\hat{\mathbf{P}}$ of UE and VAs

Calculate the residual vector $\mathbf{w}$ when the measurement matrix is $\hat{\mathbf{H}}$ according to (27);
Get the residual matrix $\mathbf{W} = \mathbf{w}\mathbf{w}^T$;
Obtain the sub-optimal lower bound $d^*(\varepsilon_A) = -\mathbf{1}^T\boldsymbol{\nu}^*$ with the error threshold ε_A according to (38) - (42);
Set the mismatch judgment threshold $\eta = d^*$;
Initialize $\mathcal{B}_k = 0, \mathcal{C} = 0, \mathbf{s} = \mathbf{0}, k = 0$
while $|\mathcal{C}| < 2(T + M)$ **do**
    Randomly select $m(m < n)$ measurements y_i from measurement set $\mathcal{Y}$ to form a subset $\mathcal{B}_k$;
    for $i = 1$ *to* N **do**
        if $y_i \in \mathcal{B}_k$ **then**
            $z_i = 1$;
        else
            $z_i = -1$; % determine the selection vector of subset
    $r_{\mathcal{B}_k} = ({\mathbf{z}_{\mathcal{B}_k}}^T + 1)^T\mathbf{W}(\mathbf{z}_{\mathcal{B}_k} + 1)/(4|\mathcal{B}_k|)$; % average of squared sum of residual of measurements in $\mathcal{B}_k$
    if $r_{\mathcal{B}_k} \leq \eta$ **then**
        $\mathcal{C} = \mathcal{C} \cup \mathcal{B}_k$; % put the candidate measurement into $\mathcal{C}$
    else
        for *each measurement in the subset* $\mathcal{B}_k$ **do**
            $s_i \leftarrow s_i + 1$; % the number of times measurement y_i is included in mismatch subsets plus one
        if $s_i \geq l$ **then**
            delete measurement y_i from $\mathcal{Y}$;
    $k \leftarrow k + 1$; % start another round of selection until $|\mathcal{C}|$ reaches threshold
if $y_i \in \mathcal{C}$ **then**
    $\boldsymbol{\alpha}_i = 1$;
else
    $\boldsymbol{\alpha}_i = 0$;
$\boldsymbol{\Phi} = \boldsymbol{\alpha}\boldsymbol{\alpha}^T$; %mismatch alleviation matrix
$\hat{\mathbf{X}} = (\hat{\mathbf{H}}^T\hat{\mathbf{H}})^{-1}\hat{\mathbf{H}}^T\boldsymbol{\Phi}^T\mathbf{Y}$; %modified correction matrix
return mismatch alleviated set $\mathcal{C}$ and estimated positions $\hat{\mathbf{P}}$ of UE and VAs.

In the RS-subset algorithm, a new measurement set is formed by a randomly selected subset of measurements with small residuals, whose elements are used to locate VAs and the UE. Therefore, the RS-Subset algorithm can quickly find a sub-optimal solution compared to the brute-force search. The probability that a randomly selected subset contains no mismatch measurements is positively correlated to the ratio of the mismatched pair in the data association results. Thus, finding this subset has low computational complexity when the number of mismatched pairs is small. On the contrary, when the mismatch problem is severe, the probability of obtaining a so-called clean subset in a single selection is slight, and the time expectation of finding a clean subset at the required scale among the total selection number becomes larger. In addition, the accuracy of the solution to this algorithm is less than that of the global optimal solution due to the duality gap between the original problem and the dual problem. This algorithm is thus better suited to scenarios with constrained computational resources.

C. Constraint Relaxation-Based Mismatch Alleviation

The RS-subset algorithm proposed in IV-B can improve the positioning accuracy. Because of the random method used in the algorithm, the performance is not always stable due to different ratios of mismatched pairs. Thus, in this subsection, we propose another mismatch alleviation algorithm based on constraint relaxation (CR) that can obtain a stable near-optimal solution. While retaining all measurements, we relax the range of values of all α_i to $[0, 1]$, which can then be used as weights for the original measurements. To retain the subset size constraint from (31), in the relaxed problem, we constrain the sum of weights to be u.

Therefore, problem (29) is relaxed as

$$\min_{\boldsymbol{\alpha}} \quad \boldsymbol{\alpha}^T\mathbf{W}\boldsymbol{\alpha} \tag{44}$$

$$\text{s.t.} \quad 0 \leq \alpha_i \leq 1, \quad \forall i \in \{1, ..., N\}, \tag{45}$$

$$\sum_{i=1}^{N} \alpha_i = u, \tag{46}$$

which is a convex quadratic program problem with inequality constraints. The optimal solution to this problem exists at the extreme point of an interval due to inequality constraints; it is therefore challenging to provide the analytical solution directly. We solve problem (44) using the barrier method combined with Newton's method, which is suitable for quadratic problem and has a feasible solution and polynomial complexity.

The barrier function for problem (44) is

$$\phi_B(\boldsymbol{\alpha}) = -\sum_{i=1}^{n} \log(1 - \alpha_i) - \sum_{i=1}^{n} \log(\alpha_i). \tag{47}$$

Problem (44) with constraints is approximately formulated as

$$\min_{\boldsymbol{\alpha}} \quad h(\boldsymbol{\alpha}) = t_B\boldsymbol{\alpha}^T\mathbf{W}\boldsymbol{\alpha} + \phi_B(\boldsymbol{\alpha}) \tag{48}$$

$$\text{s.t.} \quad \sum_{i=1}^{N} \alpha_i = u, \quad \forall i \in \{1, ..., N\}, \tag{49}$$

where $t_B > 0$.

We can obtain Newton's descent direction $\Delta\boldsymbol{\alpha}$ and decrement λ^2 by solving the Karush-Kuhn-Tucker (KKT) equations, which are described in Appendix A.

After determining $\boldsymbol{\alpha}$ by solving the above optimization problem, we can similarly find the mismatch alleviation matrix $\boldsymbol{\Phi}$ and estimate the positions $\hat{\mathbf{P}}$ of UE and VAs according to (43) and (23).

Algorithm 2: CR (constraint relaxation) algorithm.

Input: Estimated measurement matrix $\hat{\mathbf{H}}$, number of measurements N, constraint on the sum of weights u, parameters ε_B, ϵ , and ρ

Output: Modified correction matrix $\mathbf{X}$

1 Calculate the residual vector $\mathbf{w}$ when the measurement matrix is $\hat{\mathbf{H}}$ according to (27);
2 Get the residual matrix $\mathbf{W} = \mathbf{w}\mathbf{w}^T$
3 **Initialize**
$\boldsymbol{\alpha}_i{}^{(0)} = u/N, \beta = 1, \Delta\boldsymbol{\alpha}^* = 0, \lambda^2 = 0, t_B^{(0)} = 1$
4 **if** $2N/t_B \geq \varepsilon_B$ **then**
5 **repeat**
6 $\boldsymbol{\alpha} := \boldsymbol{\alpha} + \beta\Delta\boldsymbol{\alpha}^*$;
7 update step length β of inner iteration by backtracking line search;
8 Compute the Newton descent direction $\Delta\boldsymbol{\alpha}^*$ and Newton decrement λ^2 according to (50)-(51), (57) and (58);
9 **until** $\lambda^2/2 \leq \epsilon$;
10 Update the vector $\boldsymbol{\alpha}_{new} = \boldsymbol{\alpha}$;
11 $t_B := \rho t_B$;
12 $\boldsymbol{\Theta} = \boldsymbol{\alpha}_{new}\ \boldsymbol{\alpha}_{new}{}^T$; % determine the mismatch alleviation matrix $\boldsymbol{\Theta}$ of mismatched observation matrix $\mathbf{H}$
13 $\hat{\mathbf{X}} = (\hat{\mathbf{H}}^T\hat{\mathbf{H}})^{-1}\hat{\mathbf{H}}^T\boldsymbol{\Theta}\mathbf{Y}$; %modified correction matrix
14 Compute and return the estimated positions $\hat{\mathbf{P}}$ of UE and VAs.

The detailed process appears in Algorithm 2. In the inner iterations, Newton's method is used to obtain the central point vector $\boldsymbol{\alpha}$ corresponding to each β (Line 5 - 9). The step length is obtained by backtracking the line search (Line 7) [52]. The descent direction and decrement is computed based on the first-order derivative vector and the second-order derivative matrix (Line 8). At each outer iteration (Line 4 - 11), we calculate a new $\boldsymbol{\alpha}$ corresponding to the current t_B starting from the previously computed $\boldsymbol{\alpha}$ until t_B, increased by the scale factor ρ, surpasses the threshold. The final obtained $\boldsymbol{\alpha}_{new}$ is the measurement weight that minimizes the weighted squared sum of the residual of all measurements.

The CR algorithm can obtain the global near-optimal solution of the original problem. However, the first- and second-order derivatives must be calculated, as must the inverse of the matrix. Subsequent positioning also needs to use all weighted measurements. Thus, this algorithm is computationally intensive and its complexity grows along with the number of measurements. Compared with the RS-subset algorithm proposed in the previous section, the computational load of the CR-based algorithm is not sensitive to the ratio of mismatched pairs. Therefore, this algorithm is more suitable for scenarios with sufficient computational resources and high requirements for positioning performance.

D. Processing of non-Gaussian impairments

Measurements provided by channel estimators not only contain Gaussian measurement noise (related to system parameters and channel conditions), but also missed detection (a measurement related to a VA is not detected) and false alarms/clutter [44], [53]–[55].

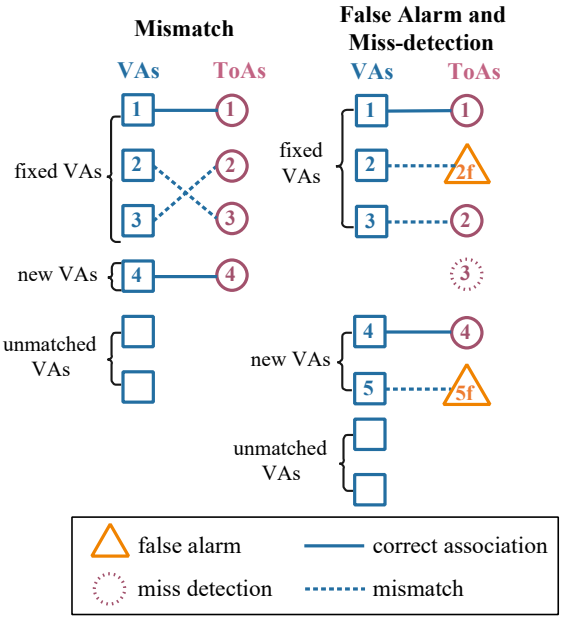

Fig. 2. Example of the false alarm and miss-detection. Blue squares and pink circles indicate VAs and measurements separately. The blue solid lines and dashed lines indicate the correct data association and mismatch, respectively. The false alarm is equivalent to the mismatch.

For miss-detection, the unobserved measurements and their corresponding VAs do not participate in the UE's positioning. So, the miss-detection only reduces the number of measurements and does not affect the positioning results. In addition, the false alarm in data association can be expressed as the association of VA with noise that is mistaken as a measurement. Therefore, the false alarm can also be equated to a mismatch, meaning that the proposed mismatch alleviation algorithms can also handle the false alarm. An example of the false alarm and miss-detection is depicted in Fig. 2. We assume the measurements are arranged by order of associated VAs, i.e., the i-th VA should be associated with the i-th measurement $\tau_t^{(i)}$ at epoch t. Blue squares and pink circles indicate VAs and measurements separately. The blue solid lines and dashed lines indicate the correct data association and mismatch, respectively. A false alarm may be associated with a fixed VA (e.g., fixed VA 2 associated with false alarm 2f), or generate a new VA (e.g., new VA 5 generated by false alarm 5f). The position estimate of the new VA generated by a false alarm cannot converge (i.e., the latter case), so we can exclude it by estimate quality control. For the former case, the false alarm is equivalent to the mismatch shown in the left picture of Fig. 2.

Furthermore, for clutter measurement, the estimated position of the corresponding VA may not converge, and we can exclude the non-converging VA from the UE positioning through the estimate quality control of the VA's position. Therefore, the proposed algorithms are directly applicable to real-world data with non-Gaussian impairments.

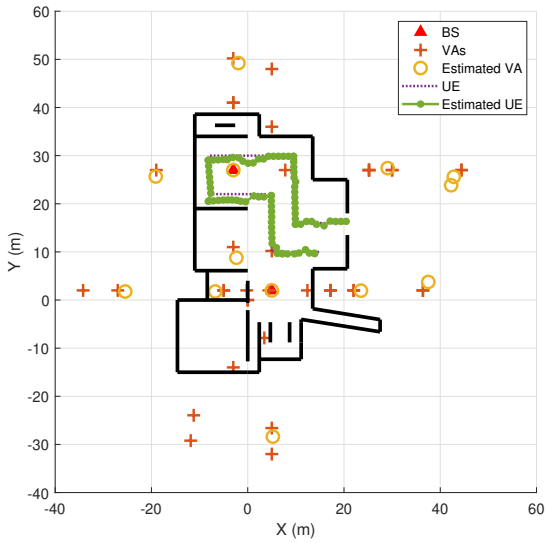

Fig. 3. Simulated indoor scenario with two fixed BSs and a moving UE. UE is moving on the track as indicated in purple dashed line. The green line indicates the UE position estimations of proposed multipath-assisted positioning method. First- and second-order VAs are used in the simulations. For ease of representation, we only mark the true positions of first-order VAs, which are indicated by red crosses. Orange circles represent estimated VAs. The proposed MSC-MAP method can estimate convergent VAs' positions and UE's trajectory with high accuracy.

V. Performance Evaluation

A. Performance of MSC-MAP

We assess the performance of the proposed MSC-MAP algorithm via a 2-D scenario simulation (see Fig. 3), with a moving UE and two static BSs. The simulation parameters are decided according to the typical indoor pedestrian scenario. The UE is moving at a speed about 1 m/s along a polyline trajectory around the building, indicated by the green dotted line. The entire trajectory is about 85 m long. The sampling frequency of ToA measurements is 1 Hz, and the interval of measurement epoch is 1 s. At each epoch, the two BSs transmit signals at a bandwidth of 100 MHz with a carrier frequency of $f_c = 2.4$ GHz, which is received and processed by the UE. For measured signals, the ToA estimation noises are generated according to [56] with sub-carrier frequency $f_{sc} = 30$ kHz. The performance is evaluated through Monte-Carlo simulations with 5000 independent runs.

As mentioned in Section II, the VA position of the multipath is the mirror point of the source point (e.g., the BS) against the reflecting surface. Due to attenuation through every reflection of the transmitted signal, we only consider at most second-order VAs in the simulation. The number of the first- and second-order VAs are 26 and 396 separately. For convenience, we mark all first-order VAs with red crosses in Fig. 3.

Fig. 3 depicts the estimated positions of the UE compared with the UE track and VAs compared with ideal VA positions. The green line indicates the UE position estimations. The VAs are denoted by orange circles. For scatterers or non-specular reflections, the positions of corresponding VAs may vary with different UE locations. The estimated location of non-specular VAs may therefore not converge, and specular VAs can be identified through convergence evaluation methods. In this scenario, results demonstrate that the proposed MSC-MAP can estimate convergent VAs' positions and UE's trajectory with high accuracy.

The performance for positioning VAs is further pictured in Fig. 4, displaying (a) the number of fixed VAs and (b) the median positioning error of fixed VAs versus the signal-to-noise ratio (SNR) at different bandwidths, respectively. We define a VA as fixed when the posterior residual of measurements corresponding to the VA is less than a pre-defined threshold. In the simulation, the residual threshold for a fixed VA is 0.1 m. Fig. 4(a) shows that the number of fixed VAs increases first before becoming stable, as the number of visible VAs is limited in the UE trajectory. The number of estimated convergent VAs is about 11. We use the median to evaluate the positioning error of fixed VAs to exclude the effects of unfixed VAs. As presented in Fig. 4(b), when the SNR is low, the number of VAs that are fixed is small. The observation quality of such VAs is high, however, leading the positioning accuracy of fixed VAs to be high as well. While the quantity of fixed VAs rises with SNR, there are instances of poor quality among them, thereby influencing the precision of positioning results. The accuracy of ToA measurements steadily enhances with increasing SNR, leading to a gradual enhancement in the quality of fixed VAs and a reduction in positioning errors.

The UE position can also be estimated well using the MSC-MAP, as indicated in Fig. 4(c). The MSE of the UE position is below 0.2 m for most bandwidth settings when the SNR is greater than 16 dB. The MSE mostly remains stable due to the estimated UE position residing on a circle, centered at a VA with a radius defined by a ToA measurement. Consequently, the accuracy of VA positioning significantly impacts the UE's positioning outcome. The estimated VA positions used for UE positioning contain error, further leading to a lower bound for the UE-positioning MSE.

Fig. 5 plots the minimum observation epochs for a different number of unknown VAs. Any integer epoch and number greater than the minimum can satisfy the constraint. As shown in the Fig. 5, the number of minimum observation epochs decreases with the number of known VAs. With insufficient known VA, the higher the number of unknown VA, the more observation epoch is required.

B. Performance of Proposed Mismatch Alleviation Methods

This section first demonstrates the impact of a mismatch on positioning performance and next evaluates the proposed two mismatch alleviation algorithms (i.e., the RS-subset algorithm and the CR algorithm). The simulation scenario and signal parameters are the same as in the prior section.

1) Analysis of mismatch effect on positioning performance: We first evaluate the percentage of mismatches using the data association method in [30]. For the sake of comparison, we also consider the low sampling frequency scenario of 0.5 Hz. Thus, we use two different pace settings: short pace (SP) and long pace (LP), whose step sizes are 1 m and 2 m, respectively. Fig. 6 illustrates the average mismatch rate for the two settings.

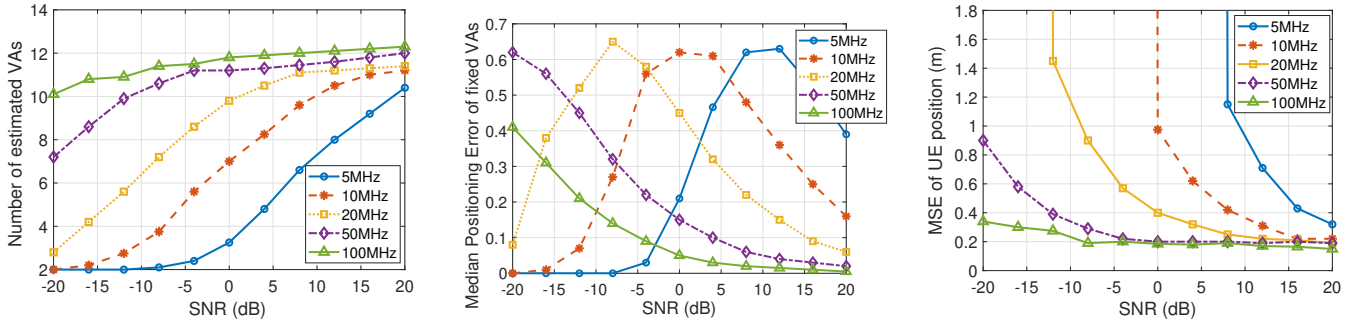

(a) (b) (c)

Fig. 4. Results for positioning VAs and UE using MOC positioning versus SNR with different bandwidths: (a) average number of estimated VAs; (b) median positioning error of fixed VAs; (c) MSE of estimated UE position. In (a) and (b), the number of estimated VAs grows and the median positioning error of VAs declines with SNR. However, with small bandwidth, the positioning error increases with the number of VA when VA's number is less than 8. In (c), the MSE of the UE position declines with SNR.

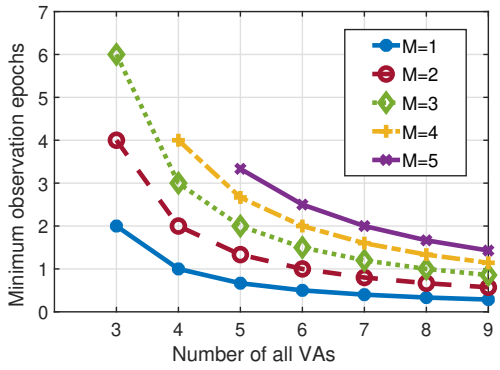

Fig. 5. Minimum observation epochs to achieve VA-assisted positioning and make estimated positions of UE and unknown VAs converge for the different number of unknown VAs. M represents the number of unknown VAs and vertical coordinate represents the number of minimum observation epochs. Different colors of curves represent the minimum observation epochs for different numbers of unknown VAs, which decreases with the number of known VAs.

In SP and LP, the average mismatch rates are 22.1% and 33.5% obtained by averaging over the 100 simulation runs. This result reveals that the mismatched association accounts for a large proportion of all measurements. As the step size increases, the mismatch rate also rises.

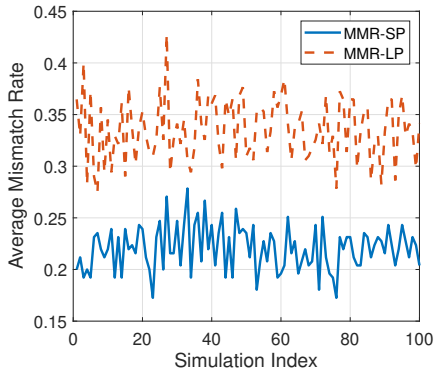

Fig. 6. The average mismatch rate for two different pace settings. The mismatched association accounts for a large proportion of all measurements, and the mismatch rate increases with the step size.

To assess the effect of mismatch, Fig. 7(a) shows the cumulative distribution function (CDF) of positioning error when mismatched measurements account for 16%, 25%, 33%, and 42%. Positioning performance deteriorates rapidly as the percentage of the mismatch increases. Specifically, when 42% of the associated measurements are mismatched, the 1-sigma (68.27%) positioning errors surpass 3 meters and may extend to as much as 6.5 meters. Therefore, as described in Section IV, the data association mismatch can significantly impede positioning performance. Consequently, our simulation reaffirms the critical importance of addressing data association mismatches in multipath-assisted positioning.

2) Performance of RS-subset algorithm: In the simulation scenario, the number of first-order VAs is 26, and the number of second-order VAs is 396. The number of visible VAs fluctuates around 50 in each epoch. Due to the MOC, we set the target size of the subset for positioning to 54. For each choice, the size of the randomly selected subset is set to 4.

As illustrated in Fig. 7(b), the RS-subset algorithm can significantly enhance the positioning accuracy compared to scenarios without data mismatch alleviation. To explore this improvement, we experimented with four distinct parameter settings for the mismatch proportion R_{mm} and the error threshold ε_A. Notably, when one-quarter of measurements are mismatched, and ε_A is set at 1.0, the 1-sigma positioning error remains below 0.8 meters. Across all four cases, varying in mismatch proportions, the RS-subset algorithm consistently reduces the positioning error to one-third of that observed in scenarios without mismatch alleviation.

Furthermore, within the RS-subset algorithm, we have the flexibility to manage the upper limit of random selection error by fine-tuning the parameter ε_A. Decreasing ε_A enhances positioning precision, albeit at the cost of slightly increased computational complexity. Additionally, it's important to note that the runtime of the RS-subset algorithm scales with the number of measurements m contained within each subset.

3) Performance of CR algorithm: To confirm the elimination performance of the CR algorithm, we use empirical values as $\alpha = 0.01$, $\beta = 0.5$, $\epsilon = 10^{-5}$, $\rho = 15$. Fig. 7(c) presents the CDF of the positioning error for the CR algorithm versus the original method without mismatch elimination. The

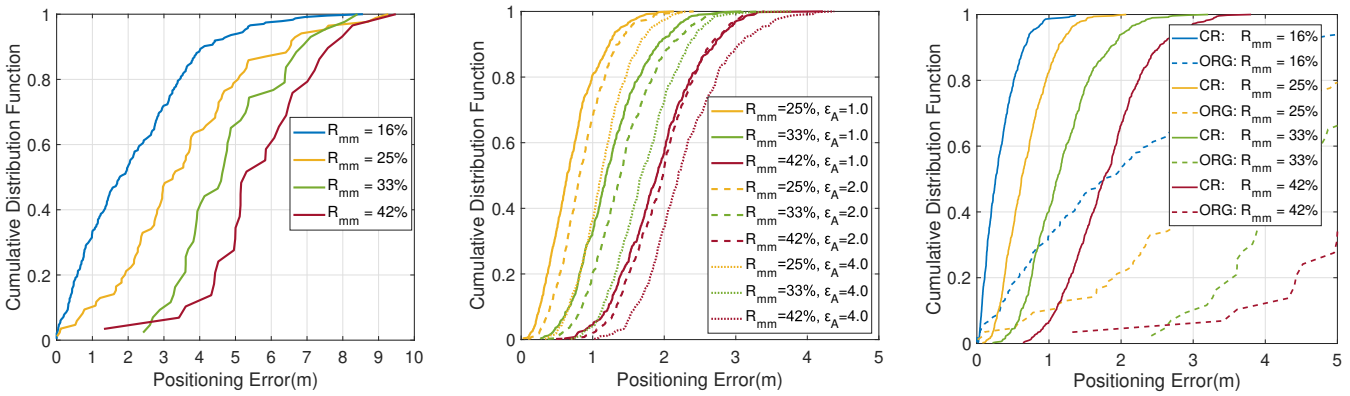

Fig. 7. Results for mismatch analysis and alleviation: CDF of positioning error with different mismatch proportions R_{mm} (a) of measurement in original data association; (b) for random selection in RS-subset algorithm with different error thresholds ε_A; (c) for CR algorithm (indicated by solid lines) compared with the original algorithm without mismatch alleviation (indicated by dashed lines). In (a), positioning performance deteriorates rapidly as the percentage of the mismatch increases. In (b) and (c), both mismatch alleviation algorithms can substantially reduce the positioning error. RS-subset algorithm can control the positioning accuracy by adjusting ε_A. The CR algorithm has better alleviation performance.

CR algorithm's positioning error falls to nearly one-quarter of that of the original method, revealing the effectiveness of this algorithm in eliminating the impact of a mismatch.

The CR algorithm also performs similarly to the RS-subset algorithm for the error threshold $\varepsilon_A = 1.0$. While the RS-subset algorithm may not attain the optimal solution, it excels in striking a balance between positioning performance and runtime through the flexible adjustment of ε_A. In contrast, the CR algorithm distinguishes itself by excelling in mismatch elimination, resulting in more accurate positioning as it approaches a near-optimal solution.

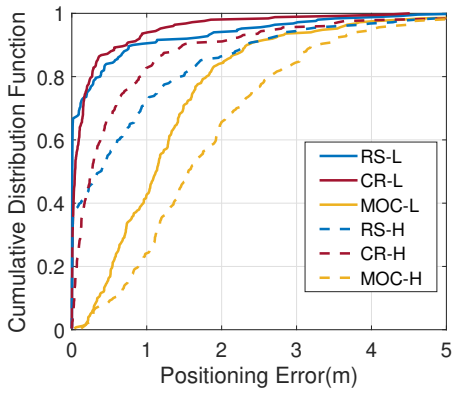

Fig. 8. Result of performance under non-Gaussian impairments. Two different parameter settings are considered: (1) H: high SNR with false alarm probability 0.1 and miss-detection probability 0.2; (2) L: low SNR with false alarm probability 0.2 and miss-detection probability 0.3. The proposed two algorithms are both effective in improving the positioning performance in a scenario where false alarms and miss-detection exist.

4) Performance under non-Gaussian impairments: Then, we verify the performance of the proposed mismatch alleviation algorithms in the scenario with false alarms and miss-detection. We consider two different parameter settings. One is high SNR with false alarm probability 0.1 and miss-detection probability 0.2. The other is low SNR with false alarm probability 0.2 and miss-detection probability 0.3. The high SNR and low SNR are denoted as H and L, respectively, in Fig. 8. As demonstrated in Fig. 8, the RS-subset algorithm and CR algorithm are both effective in improving the positioning performance in a scenario where false alarms and miss-detection exist. The result coincides with our analysis of treating non-Gaussian impairments as mismatches.

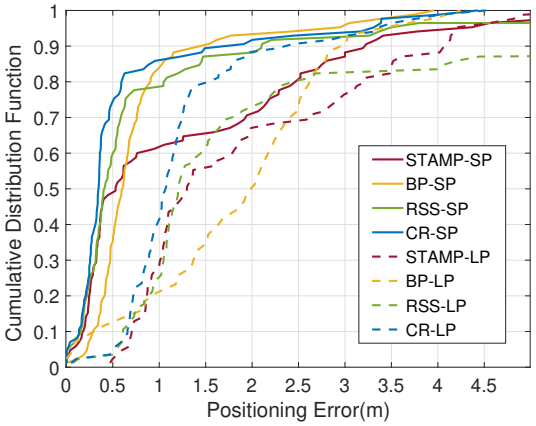

Fig. 9. Result of performance comparison with state-of-the-art methods: CDF of positioning error of RS-subset, CR, STAMP, and BP-SLAM. The solid and dashed lines represent SP and LP, respectively. The RS-subset and CR can both substantially improve positioning performance by solving the mismatch problem in both settings. The positioning performance of BP-SLAM decreases sharply when the step size increases.

5) Comparison with state-of-the-art methods: Next, we compare the CDF of the positioning error of our proposed algorithm with those of STAMP [30] and BP-SLAM [35], in which the hard data association method and probabilistic data association method are used, respectively. We also consider two different pace settings, dubbed SP and LP. We set $\varepsilon_A = 2.0$ for the RS-subset algorithm with a slightly weaker alleviation performance compared to CR algorithm. Fig. 9 shows the CDF of the positioning error of the BP-SLAM, STAMP, and the proposed two mismatch alleviation algorithms. The RS-subset and CR algorithms reduce the positioning error of STAMP algorithm by 69.0% and 77.3% for the SP, and the reductions are 23.8% and 44.8% for the

TABLE II
AVERAGE RUNTIME PER SIMULATION RUNS

STAMP	BP-SLAM	RS-subset	CR
2.88 s	48.38 s	2.94 s	3.29 s

LP. For the BP-SLAM, the positioning performance is stable when the step size is small. The proposed two algorithms both slightly improve the positioning performance, reducing the 1-sigma positioning error from 0.74 m to 0.42 m and 0.57 m, respectively. However, when the step size increases, the correlation between adjacent sampling points weakens, resulting in a sharp decline in the positioning performance of BP-SLAM, with a positioning error as high as 2.33 m. The two proposed algorithms improve the positioning performance by 27.5% and 47.4%.

Therefore, the following further conclusions can be drawn: (i) The proposed two mismatch alleviation algorithms can substantially improve positioning performance by solving the mismatch problem in both settings. (ii) BP-SLAM requires a strong spatial correlation of adjacent sampling points. The correlation weakens when the step size increases. Hence, BP-SLAM and other probabilistic data association methods are unsuitable for scenarios with sparse sampling points. However, the proposed MSC estimator can maintain the constraint between sampling points, thus keeping a stable positioning performance when the step size increases.

In addition, we compare the complexity of the four methods using the average time per simulation run (average over 100 simulation runs), shown in Table II. The simulations are implemented by MATLAB R2017b on an Intel(R) Core (TM) i5-8265U @1.60GHz with 8 GB RAM. It is seen from Table II that the complexity of STAMP, RS-subset, and CR is similar. The addition of mismatch alleviation adds little to no computation time. In addition, due to complicated probability calculation, the complexity of BP-SLAM is very high, and the runtime is about 15 times of the other three algorithms. Therefore, BP-SLAM is challenging to achieve real-time positioning in terms of implementation.

VI. CONCLUSION

We propose a novel ToA-based multipath-assisted real-time and low computation complexity positioning algorithm, namely MSC-MAP, taking advantage of delay measurements of reflected signals as additional spatial observations. We model the propagation paths of reflected signals as VAs, and estimate the positions of UE and VAs via a MSC estimator to deal with the insufficient observation. We use estimation quality control to find some VAs in the environment that can be used to assist positioning without using strict specular reflection assumption. Based on observation model, we analyze the MOC for the proposed estimator. Once the number of observation epochs used in a single estimating step satisfies the MOC, the converged estimations of UE's positions can be obtained.

We then propose two mismatch alleviation approximation algorithms to handle mismatches in data association. Finding the optimal mismatch alleviation matrix needs brute-force search. The proposed algorithms meet the requirement of real-time processing. Specifically, the first strategy is based on random selection. It can obtain a sub-optimal solution with light computational complexity and achieve a tradeoff between time and accuracy. The second method based on constraint relaxation can obtain a near-optimal solution, but it requires greater computational resources. For practical use, we can choose a mismatch alleviation algorithm in accordance with computational resources and levels of mismatch. The proposed algorithms are also efficient for signal with non-Gaussian impairments that are common in real-world data.

Simulation results using synthetic data show that the proposed algorithms estimate the trajectory of a moving UE with high accuracy and robustness, even when encountering a high proportion of mismatched measurements in data association. An accuracy rate below 0.2 m in the simulated scenario can be achieved using two base stations in a complex environment for an SNR greater than 16 dB with 20 MHz bandwidth. In addition, we validate that mismatched measurements indeed constitute a significant portion and evaluate their impact. Mismatch alleviation approaches can reduce the positioning error by 69% even when the percentage of mismatched measurement data is as high as 42%, significantly improving the performance of multipath-assisted positioning. Moreover, our proposed algorithms can substantially improve positioning performance when confronted with measurement mismatches while incurring minimal additional computation time compared to existing state-of-the-art methods employing different data association techniques.

In this paper, we have not used angular measurements, which can also be accurately resolved by 5G MIMO equipment. Our future research will explore the incorporation of angle information to enhance positioning accuracy further. Additionally, it's important to note that our performance evaluations have been based on synthetic measurements, and further investigations are warranted using real-world data. Furthermore, an exciting avenue for future research lies in exploring RIS-assisted positioning.

APPENDIX A
NEWTON'S DESCENT DIRECTION AND DECREMENT

Here, we introduce the detailed derivation of Newton's descent direction and decrement.

The first-order derivative and the Hessian matrix of $h(\boldsymbol{\alpha})$ are needed. By taking partial derivatives of α_i, the first-order derivative vector of $h(\boldsymbol{\alpha})$ is

$$\nabla h(\boldsymbol{\alpha}) = \left(\frac{\partial h}{\partial \alpha_1}, \cdots, \frac{\partial h}{\partial \alpha_n} \right),$$
$$\frac{\partial h}{\partial \alpha_i} = 2t \sum_{j=1}^{n} w_{ij}\alpha_j - \frac{1}{\alpha_i - 1} - \frac{1}{\alpha_i}, \forall i \in \{1, ..., N\}. \tag{50}$$

The second-order derivative is then given by

$$\frac{\partial^2 h}{\partial {\alpha_i}^2} = 2tw_{ii} + \frac{1}{(\alpha_i - 1)^2} + \frac{1}{{\alpha_i}^2}, \quad \forall i \in \{1, ..., N\}, \tag{51a}$$

$$\frac{\partial^2 h}{\partial \alpha_i \partial \alpha_j} = 2tw_{ij}, \qquad \forall i \in \{1, ..., N\}. \tag{51b}$$

Thus, the Hessian matrix of $h(\cdot)$ is $\nabla^2 h(\boldsymbol{\alpha}) \in \mathbb{R}^{N\times N}$ with elements $\{\nabla^2 h(\boldsymbol{\alpha})\}_{i,j} = \partial^2 h/\partial {\alpha_i}^2$ if $i = j$ and $\{\nabla^2 h(\boldsymbol{\alpha})\}_{i,j} = \partial^2 h/\partial\alpha_i\partial\alpha_j$ if $i \neq j$.

According to [52], we replace problem (45) with its second-order Taylor approximation near $\boldsymbol{\alpha}$ and get

$$\begin{aligned} \min_{\boldsymbol{\alpha}} \quad & h(\boldsymbol{\alpha} + \Delta\boldsymbol{\alpha}) \\ & = h(\boldsymbol{\alpha}) + \nabla h(\boldsymbol{\alpha})^T \Delta\boldsymbol{\alpha} + \frac{1}{2}\Delta\boldsymbol{\alpha}^T \nabla^2 h(\boldsymbol{\alpha}) \Delta\boldsymbol{\alpha} \quad (52) \\ \text{s.t.} \quad & \mathbf{1}^T(\boldsymbol{\alpha} + \Delta\boldsymbol{\alpha}) = u. \quad (53) \end{aligned}$$

Next, we have the following KKT conditions:

$$\begin{cases} \nabla_{\Delta\boldsymbol{\alpha}} L(\boldsymbol{\alpha} + \Delta\boldsymbol{\alpha}, \nu) & (54) \\ = \nabla^2 h(\boldsymbol{\alpha}) \cdot \Delta\boldsymbol{\alpha} + \nabla h(\boldsymbol{\alpha}) + \nu \cdot \mathbf{1}^T = 0, & \\ \mathbf{1}^T \cdot \Delta\boldsymbol{\alpha} = \mathbf{1}^T(\boldsymbol{\alpha} + \Delta\boldsymbol{\alpha}) - \mathbf{1}^T \cdot \boldsymbol{\alpha} = 0, & (55) \end{cases}$$

where ν is the Lagrange multiplier associated with problem (53).

By solving (54), we have

$$\Delta\boldsymbol{\alpha}^* = -\nabla^2 h(\boldsymbol{\alpha})^{-1}[\nabla h(\boldsymbol{\alpha}) + \nu^* \cdot \mathbf{1}^T]. \tag{56}$$

We next substitute (56) into (55) to obtain the Lagrange multiplier:

$$\nu^* = -\frac{\mathbf{1}^T \cdot \nabla^2 h(\boldsymbol{\alpha})^{-1} \cdot \nabla h(\boldsymbol{\alpha})}{\mathbf{1}^T \cdot \nabla^2 h(\boldsymbol{\alpha})^{-1} \cdot \mathbf{1}}. \tag{57}$$

Then, $\Delta\boldsymbol{\alpha}^*$ can be calculated by substituting (57) into (56).

The Newton decrement is [52]

$$\begin{aligned} \lambda^2 &= \Delta\boldsymbol{\alpha}^T \cdot \nabla^2 h(\boldsymbol{\alpha}) \cdot \Delta\boldsymbol{\alpha} \\ &= [\nabla h(\boldsymbol{\alpha}) + \nu^* \cdot \mathbf{1}^T]^T \cdot [\nabla h(\boldsymbol{\alpha})^{-1}]^T \cdot [\nabla h(\boldsymbol{\alpha}) + \nu^* \cdot \mathbf{1}^T]. \end{aligned} \tag{58}$$

REFERENCES

[1] H. Chen, H. Sarieddeen, T. Ballal, H. Wymeersch, M.-S. Alouini, and T. Y. Al-Naffouri, "A tutorial on terahertz-band localization for 6g communication systems," *IEEE Communications Surveys & Tutorials*, vol. 24, no. 3, pp. 1780–1815, 2022.

[2] W. Shao, H. Luo, F. Zhao, H. Tian, S. Yan, and A. Crivello, "Accurate indoor positioning using temporal-spatial constraints based on Wi-Fi fine time measurements," *IEEE Internet Things J.*, vol. 7, no. 11, pp. 11 006–11 019, 2020.

[3] Y. Yu, R. Chen, L. Chen, X. Zheng, D. Wu, W. Li, and Y. Wu, "A novel 3-D indoor localization algorithm based on BLE and multiple sensors," *IEEE Internet Things J.*, vol. 8, no. 11, pp. 9359–9372, 2021.

[4] S. Zhao, X.-P. Zhang, X. Cui, and M. Lu, "A new TOA localization and synchronization system with virtually synchronized periodic asymmetric ranging network," *IEEE Internet Things J.*, vol. 8, no. 11, pp. 9030–9044, 2021.

[5] J. A. del Peral-Rosado, R. Raulefs, J. A. López-Salcedo, and G. Seco-Granados, "Survey of cellular mobile radio localization methods: From 1G to 5G," *IEEE Commun. Surveys Tuts.*, vol. 20, no. 2, pp. 1124–1148, 2017.

[6] H.-J. Shao, X.-P. Zhang, and Z. Wang, "Efficient closed-form algorithms for aoa based self-localization of sensor nodes using auxiliary variables," *IEEE Trans. Signal Process.*, vol. 62, no. 10, pp. 2580–2594, 2014.

[7] Z. Wang, J.-A. Luo, and X.-P. Zhang, "A novel location-penalized maximum likelihood estimator for bearing-only target localization," *IEEE Trans. Signal Process.*, vol. 60, no. 12, pp. 6166–6181, 2012.

[8] A. Elzanaty, A. Guerra, F. Guidi, and M.-S. Alouini, "Reconfigurable intelligent surfaces for localization: Position and orientation error bounds," *IEEE Trans. Signal Process.*, vol. 69, pp. 5386–5402, 2021.

[9] S. Zhao, X.-P. Zhang, X. Cui, and M. Lu, "Optimal two-way TOA localization and synchronization for moving user devices with clock drift," *IEEE Trans. Veh. Technol.*, vol. 70, no. 8, pp. 7778–7789, 2021.

[10] Y. Han, Y. Shen, X.-P. Zhang, M. Z. Win, and H. Meng, "Performance limits and geometric properties of array localization," *IEEE Trans. Inf. Theory*, vol. 62, no. 2, pp. 1054–1075, 2015.

[11] M. Compagnoni, A. Pini, A. Canclini, P. Bestagini, F. Antonacci, S. Tubaro, and A. Sarti, "A geometrical–statistical approach to outlier removal for TDOA measurements," *IEEE Trans. Signal Process.*, vol. 65, no. 15, pp. 3960–3975, 2017.

[12] Z. Li, Z. Tian, M. Zhou, Z. Zhang, and Y. Jin, "Awareness of line-of-sight propagation for indoor localization using hopkins statistic," *IEEE Sens. J.*, vol. 18, no. 9, pp. 3864–3874, 2018.

[13] I. Podkurkov, G. Seidl, L. Khamidullina, A. Nadeev, and M. Haardt, "Tensor-based near-field localization using massive antenna arrays," *IEEE Trans. Signal Process.*, vol. 69, pp. 5830–5845, 2021.

[14] D. Feng, J. Peng, Y. Zhuang, C. Guo, T. Zhang, Y. Chu, X. Zhou, and X.-G. Xia, "An adaptive IMU/UWB fusion method for NLOS indoor positioning and navigation," *IEEE Internet Things J.*, vol. 10, no. 13, pp. 11 414–11 428, 2023.

[15] R. K. Martin, A. S. King, J. R. Pennington, R. W. Thomas, R. Lenahan, and C. Lawyer, "Modeling and mitigating noise and nuisance parameters in received signal strength positioning," *IEEE Trans. Signal Process.*, vol. 60, no. 10, pp. 5451–5463, 2012.

[16] D. Jin, F. Yin, A. M. Zoubir, and H. C. So, "Exploiting sparsity of ranging biases for NLOS mitigation," *IEEE Trans. Signal Process.*, vol. 69, pp. 3782–3795, 2021.

[17] G. Dumphart, R. Kramer, R. Heyn, M. Kuhn, and A. Wittneben, "Pairwise node localization from differences in their UWB channels to observer nodes," *IEEE Trans. Signal Process.*, 2022.

[18] Z. Wu, Y. Li, X. Meng, X. Lv, and Q. Guo, "A minimum joint error entropy-based localization method in mixed LOS/NLOS environments," *IEEE Internet Things J.*, pp. 1–1, 2023.

[19] N. Rogel, D. Raphaeli, and O. Bialer, "Time of arrival and angle of arrival estimation algorithm in dense multipath," *IEEE Trans. Signal Process.*, vol. 69, pp. 5907–5919, 2021.

[20] K. Witrisal, P. Meissner, E. Leitinger, Y. Shen, C. Gustafson, F. Tufvesson, K. Haneda, D. Dardari, A. F. Molisch, A. Conti *et al.*, "High-accuracy localization for assisted living: 5G systems will turn multipath channels from foe to friend," *IEEE Signal Process. Mag.*, vol. 33, no. 2, pp. 59–70, 2016.

[21] R. Mendrzik, H. Wymeersch, G. Bauch, and Z. Abu-Shaban, "Harnessing NLOS components for position and orientation estimation in 5G millimeter wave mimo," *IEEE Trans. Wireless Commun.*, vol. 18, no. 1, pp. 93–107, 2018.

[22] J. Borish, "Extension of the image model to arbitrary polyhedra," *J. Acoust. Soc. Am.*, vol. 75, no. 6, pp. 1827–1836, 1984.

[23] M. Z. Win, Y. Shen, and W. Dai, "A theoretical foundation of network localization and navigation," *Proc. IEEE*, vol. 106, no. 7, pp. 1136–1165, 2018.

[24] H. Naseri and V. Koivunen, "Cooperative simultaneous localization and mapping by exploiting multipath propagation," *IEEE Trans. Signal Process.*, vol. 65, no. 1, pp. 200–211, 2016.

[25] M. Kreković, I. Dokmanić, and M. Vetterli, "Shapes from echoes: uniqueness from point-to-plane distance matrices," *IEEE Trans. Signal Process.*, vol. 68, pp. 2480–2498, 2020.

[26] E. Leitinger and F. Meyer, "Data fusion for multipath-based SLAM," in *2020 54th Asilomar Conf. Signals Syst. Comput.* IEEE, 2020, pp. 934–939.

[27] J. Kulmer, E. Leitinger, S. Grebien, and K. Witrisal, "Anchorless cooperative tracking using multipath channel information," *IEEE Trans. Wireless Commun.*, vol. 17, no. 4, pp. 2262–2275, 2018.

[28] Y. Wang, W. Ren, L. Cheng, and J. Zou, "A grey model and mixture gaussian residual analysis-based position estimator in an indoor environment," *Sensors*, vol. 20, no. 14, p. 3941, 2020.

[29] C.-H. Park and J.-H. Chang, "Robust localization based on ML-type, multi-stage ML-type, and extrapolated single propagation UKF methods under mixed LOS/NLOS conditions," *IEEE Trans. Wireless Commun.*, vol. 19, no. 9, pp. 5819–5832, 2020.

[30] L. Li and J. L. Krolik, "Simultaneous target and multipath positioning," *IEEE J. Sel. Topics Signal Process.*, vol. 8, no. 1, pp. 153–165, 2014.

[31] R. Amiri, S. Yerramalli, T. Yoo, M. Hirzallah, M. Zorgui, R. Prakash, and X. Zhang, "Indoor environment learning via RF-mapping," *IEEE J. Sel. Areas Commun.*, vol. 41, no. 6, pp. 1859–1872, 2023.

[32] X. Chu, Z. Lu, D. Gesbert, L. Wang, and X. Wen, "Vehicle localization via cooperative channel mapping," *IEEE Trans. Veh. Technol.*, 2021.

[33] J. Xiong, J. W. Cheong, Y. Ding, Z. Xiong, and A. G. Dempster, "Efficient distributed particle filter for robust range-only SLAM," *IEEE Internet Things J.*, vol. 9, no. 21, pp. 21 932–21 945, 2022.

[34] A. Shahmansoori, G. E. Garcia, G. Destino, G. Seco-Granados, and H. Wymeersch, "Position and orientation estimation through millimeter-wave mimo in 5G systems," *IEEE Trans. Wireless Commun.*, vol. 17, no. 3, pp. 1822–1835, 2017.

[35] E. Leitinger, F. Meyer, F. Hlawatsch, K. Witrisal, F. Tufvesson, and M. Z. Win, "A belief propagation algorithm for multipath-based SLAM," *IEEE Trans. Wireless Commun.*, vol. 18, no. 12, pp. 5613–5629, 2019.

[36] R. Mendrzik, F. Meyer, G. Bauch, and M. Z. Win, "Enabling situational awareness in millimeter wave massive MIMO systems," *IEEE J. Sel. Topics Signal Process.*, vol. 13, no. 5, pp. 1196–1211, 2019.

[37] E. Leitinger, S. Grebien, and K. Witrisal, "Multipath-based SLAM exploiting AoA and amplitude information," in *Proc. IEEE Int. Conf. Commun. Workshops*, 2019, pp. 1–7.

[38] H. Kim, K. Granström, L. Gao, G. Battistelli, S. Kim, and H. Wymeersch, "5G mmwave cooperative positioning and mapping using multi-model PHD filter and map fusion," *IEEE Trans. Wireless Commun.*, vol. 19, no. 6, pp. 3782–3795, 2020.

[39] H. Zhang and S. Y. Tan, "TOA based indoor localization and tracking via single-cluster PHD filtering," in *Proc. IEEE Global Commun. Conf.*, 2017, pp. 1–6.

[40] L. Lian, A. Liu, and V. K. Lau, "User location tracking in massive MIMO systems via dynamic variational bayesian inference," *IEEE Trans. Signal Process.*, vol. 67, no. 21, pp. 5628–5642, 2019.

[41] R. Mendrzik, H. Wymeersch, and G. Bauch, "Joint localization and mapping through millimeter wave MIMO in 5G systems," in *Proc. IEEE Global Commun. Conf.*, 2018, pp. 1–6.

[42] W. Zhang, J. Zhang, M. Bao, X.-P. Zhang, and X. Li, "Multitarget tracking based on dynamic bayesian network with reparameterized approximate variational inference," *IEEE Internet Things J.*, vol. 9, no. 13, pp. 11 542–11 559, 2022.

[43] Y. Tian, M. Liu, S. Zhang, R. Zheng, and Z. Fan, "Feature-aided passive tracking of noncooperative multiple targets based on the underwater sensor networks," *IEEE Internet Things J.*, vol. 10, no. 5, pp. 4579–4591, 2023.

[44] X. Li, E. Leitinger, A. Venus, and F. Tufvesson, "Sequential detection and estimation of multipath channel parameters using belief propagation," *IEEE Trans. Wireless Commun.*, 2022.

[45] X. Li, E. Leitinger, M. Oskarsson, K. Åström, and F. Tufvesson, "Massive MIMO-based localization and mapping exploiting phase information of multipath components," *IEEE Trans. Wireless Commun.*, vol. 18, no. 9, pp. 4254–4267, 2019.

[46] X. Li, K. Batstone, K. Åstrom, M. Oskarsson, C. Gustafson, and F. Tufvesson, "Robust phase-based positioning using massive mimo with limited bandwidth," in *2017 IEEE 28th Annual International Symposium on Personal, Indoor, and Mobile Radio Communications (PIMRC)*. IEEE, 2017, pp. 1–7.

[47] C. Gentner, M. Ulmschneider, R. Karásek, and A. Dammann, "Simultaneous localization of a receiver and mapping of multipath generating geometry in indoor environments," in *Proc. IEEE Radar Conf.* IEEE, 2021, pp. 1–6.

[48] 3GPP, "Physical channels and modulation (release 16)," *3GPP TS 38.211 Technical specification V16.1.0*, 2020.

[49] B. Sahbani and W. Adiprawita, "Kalman filter and iterative-hungarian algorithm implementation for low complexity point tracking as part of fast multiple object tracking system," in *Proc. Int. Conf. Syst. Eng. Technol.*, 2016, pp. 109–115.

[50] A. I. Mourikis and S. I. Roumeliotis, "A multi-state constraint kalman filter for vision-aided inertial navigation," in *Proc. IEEE Int. Conf. Robot. Autom.*, 2007, pp. 3565–3572.

[51] Y. Tian, A. Peng, X. Xu, and W. Zhang, "A heading estimation algorithm for wrist device assisted by sequential geomagnetic observations," *IEEE Sens. J.*, 2021.

[52] S. Boyd, S. P. Boyd, and L. Vandenberghe, *Convex optimization*. Cambridge University Press, 2004.

[53] T. L. Hansen, B. H. Fleury, and B. D. Rao, "Superfast line spectral estimation," *IEEE Trans. Signal Process.*, vol. 66, no. 10, pp. 2511–2526, 2018.

[54] D. Shutin, W. Wang, and T. Jost, "Incremental sparse bayesian learning for parameter estimation of superimposed signals," in *10th International Conference on Sampling Theory and Applications*, no. 1, 2013, pp. 6–9.

[55] B. H. Fleury, M. Tschudin, R. Heddergott, D. Dahlhaus, and K. I. Pedersen, "Channel parameter estimation in mobile radio environments using the sage algorithm," *IEEE J. Sel. Areas Commun.*, vol. 17, no. 3, pp. 434–450, 1999.

[56] W. Xu, M. Huang, C. Zhu, and A. Dammann, "Maximum likelihood TOA and OTDOA estimation with first arriving path detection for 3GPP LTE system," *Trans. Emerg. Telecommun. Technol.*, vol. 27, no. 3, pp. 339–356, 2016.

Xueting Xu received the B.S. degree from Nanjing University of Science and Technology, Nanjing, China. She is currently pursuing the Ph.D. degree in communication and information system at Xiamen University, China. Her research interests include wireless communications, multipath-assisted positioning, optimal state estimation.

Ao Peng received the M.Sc degree and the Ph.D in Communication and Information System from Xiamen University, Fujian, China, in 2011 and 2014, respectively. In 2015, he joined the School of Informatics, Xiamen University, where he is currently an Assistant Professor. His research interests including satellite navigation, indoor navigation and multi-source positioning and navigation.

Xuemin Hong (Member, IEEE) received the Ph.D. degree from Heriot-Watt University, U.K., in 2008. He is currently a Professor with the School of Informatics, Xiamen University, China. He has published one book chapter and over 60 articles in refereed journals and conference proceedings. His research interests include wireless communication networks and localization.

Yixiong Zhang (Member, IEEE) was born in Fujian, China, in 1981. He received the B.S. degree in information engineering and the Ph.D. degree in information and communication engineering from Zhejiang University, Hangzhou, China, in 2003 and 2009, respectively. In 2009, he joined the School of Information Science and Engineering, Xiamen University, Xiamen, China, where he is currently an Associate Professor. His current research interests include signal detection and parameter estimation, radar imaging, and hardware/software co-design of embedded systems.

Xiao-Ping Zhang (Fellow, IEEE) received B.S. and Ph.D. degrees from Tsinghua University, in 1992 and 1996, respectively, both in Electronic Engineering. He holds an MBA in Finance, Economics and Entrepreneurship with Honors from the University of Chicago Booth School of Business, Chicago, IL.

He is Chair Professor at Tsinghua-Berkeley Shenzhen Institute (TBSI). He has also been with the Department of Electrical, Computer and Biomedical Engineering, Toronto Metropolitan University (Formerly Ryerson University), Toronto, ON, Canada, as a Professor and the Director of the Communication and Signal Processing Applications Laboratory, and has served as the Program Director of Graduate Studies. He is cross-appointed to the Finance Department at the Ted Rogers School of Management, Toronto Metropolitan University. His research interests include image and multimedia content analysis, sensor networks and IoT, machine learning, statistical signal processing, and applications in big data, finance, and marketing.

Dr. Zhang is Fellow of the Canadian Academy of Engineering, Fellow of the Engineering Institute of Canada, Fellow of the IEEE, a registered Professional Engineer in Ontario, Canada, and a member of Beta Gamma Sigma Honor Society. He is the general Co-Chair for the IEEE International Conference on Acoustics, Speech, and Signal Processing, 2021. He is the general co-chair for 2017 GlobalSIP Symposium on Signal and Information Processing for Finance and Business, and the general co-chair for 2019 GlobalSIP Symposium on Signal, Information Processing and AI for Finance and Business. He was an elected Member of the ICME steering committee. He is Editor-in-Chief for the IEEE JOURNAL OF SELECTED TOPICS IN SIGNAL PROCESSING. He is Senior Area Editor for the IEEE TRANSACTIONS ON IMAGE PROCESSING. He served as Senior Area Editor the IEEE TRANSACTIONS ON SIGNAL PROCESSING and Associate Editor for the IEEE TRANSACTIONS ON IMAGE PROCESSING, the IEEE TRANSACTIONS ON MULTIMEDIA, the IEEE TRANSACTIONS ON CIRCUITS AND SYSTEMS FOR VIDEO TECHNOLOGY, the IEEE TRANSACTIONS ON SIGNAL PROCESSING, and the IEEE SIGNAL PROCESSING LETTERS. He was selected as IEEE Distinguished Lecturer by the IEEE Signal Processing Society and by the IEEE Circuits and Systems Society.